OCS Study
BOEMRE 2010-031

Inner-Shelf Surface Currents and Characteristic Flow Patterns in the Santa Barbara Channel

Final Technical Summary

Final Study Report

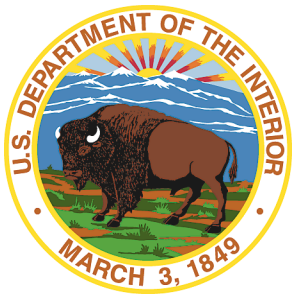

OCS Study
BOEMRE 2010-031

Inner-Shelf Surface Currents and Characteristic Flow Patterns in the Santa Barbara Channel

Final Technical Summary

Final Study Report

Author

J. Carter Ohlmann
Principal Investigator

Associated Authors

Satoshi Mitarai
Melanie Fewings

Prepared under BOEMRE Cooperative Agreement
M05AC12301
by
J. Carter Ohlmann
ERI/UCSB
University of California
Santa Barbara, CA 93106

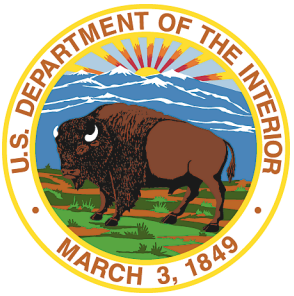

Disclaimer

This report has been reviewed by the Pacific Outer Continental Shelf Region, Bureau of Ocean Energy Management, Regulation and Enforcement, U.S. Department of the Interior and approved for publication. The opinions, findings, conclusions, and recommendations in this report are those of the authors, and do not necessarily reflect the views and policies of the Bureau of Ocean Energy Management, Regulation and Enforcement. Mention of trade names or commercial products does not constitute an endorsement or recommendation for use. This report has not been edited for conformity with Bureau of Ocean Energy Management, Regulation and Enforcement editorial standards.

Availability of Report

Extra copies of the report may be obtained from:

U.S. Dept. of the Interior
Bureau of Ocean Energy Management, Regulation and Enforcement
Pacific OCS Region
770 Paseo Camarillo
Camarillo, CA 93010
Phone: 805-389-7621

Suggested Citation

The suggested citation for this report is:

Ohlmann, J.C., 2010. Inner-shelf surface currents and characteristic flow patterns in the Santa Barbara Channel. BOEMRE OCS Study 2010-031. Earth Research Institute, University of California, Santa Barbara, California. BOEMRE Cooperative Agreement M05AC12301, 45 pages.

Table of Contents

Technical Summary

Study Title: Relationships between Inner-Shelf Surface Currents and Large-Scale Characteristic Flow Patterns in the Santa Barbara Channel

Report Title: Inner-Shelf Surface Currents and Characteristic Flow Patterns in the Santa Barbara Channel

Contract Number: M05AC12301

Sponsoring OCS Region: Pacific

Applicable Planning Area: Central and Southern California

Fiscal Years of Project Funding: FY2005-FY2010

Completion Date of the Report: October 2010

Costs: $259,685

Cumulative Project cost: $259,685

Principal Investigator: Carter Ohlmann

Key Words: ocean circulation, surface currents, inner-shelf, model validation, wave-driven currents

Background and Objectives:
During the 1990's and early 2000's, the BOEMRE sponsored the Santa Barbara Channel – Santa Maria Basin Coastal Circulation Study (SBC-SMB CCS), a large observational program aimed at improving the understanding and predictability of *large-scale* circulation patterns within the study region. A key result of the SBC-SMB CCS has been identification of the roles of local winds and a generally poleward pressure gradient in forcing surface currents (Auad and Hendershott 1997), and the definition of characteristic circulation patterns for the Channel. Patterns were initially defined as "Upwelling", "Cyclonic", "Relaxation", "Propagating Cyclones", "Flood East" and Flood West" (Harms and Winant 1998), and later reduced to "Upwelling", "Surface Convergence" and "Relaxation" (Winant et al. 2003). The characteristic patterns are extremely important because they provide a simple model for the large-scale circulation in the SBC-SMB. Data used in the SBC-SMB CCS do not resolve currents inshore of the 100 m isobath. Thus, results of that study hold for basin scale currents, and are not necessarily indicative of flows over the inner-shelf.

This project seeks to expand results of the SBC-SMB CCS by focusing on ocean circulation over the inner shelf. Particular questions to be addressed are:

- What are the characteristic patterns of circulation over the inner-shelf?
- How do the inner-shelf patterns relate to the basin-scale patterns reported by Winant et al. (2003)?
- What are the dominant forcing mechanisms?
- How well to modeled trajectories agree with observations?

Subsequent to the proposed work being funded, significant coastal ocean observing system infrastructure was deployed in the study region. The observational array attracted modeling efforts. The proposed work plan evolved to take advantage of the added measurements, and contribute to the modeling studies. Results of the funded work thus extend beyond what was proposed. In addition to the proposed statistical analysis of inner shelf flows, the work revisits the historical SBC-SMB CCS drifter data over the inner shelf in conjunction with model results, and investigates the role of wave driven flows at the surf zone interface. Manuscripts on each of these three topics (tasks) are in various stages of the publication process and comprise this final report.

Description:

The inner-shelf circulation was studied through three distinct tasks that naturally follow the successful SBC-SMB CCS.

Task 1: Lagrangian Assessment of Simulated Surface Current Dispersion in the Coastal Ocean

Model surface current trajectories computed from ROMS, a state-of-the-art ocean circulation model, were validated with historical drifter trajectories. The analysis required defining and implementing a quantitative comparison metric specific to Lagrangian data. Results show that model trajectories launched over the continental shelf throughout the SBC generally agree with observations.

Task 2: Wave-driven inner-shelf motions in Southern California

Drifting buoys that moved onshore generally appeared to decelerate as they reached the surf zone. This task tests the hypothesis that observed decelerations are a result of wave forced undertow. An undertow model gives decelerations that agree with observations. Results indicate that Eulerian observations may not necessarily capture all components of Lagrangian flows that move passive tracers.

Task 3: Circulation patterns over the inner-shelf of the Santa Barbara Channel

Relationships among moored velocity observations located on the inner-shelf were investigated. Results indicate that circulation patterns over the inner-shelf cannot be mostly explained by a few coherent statistical modes or patterns, as is the case for currents further offshore.

Significant Results:

Task 1: Lagrangian Assessment of Simulated Surface Current Dispersion in the Coastal Ocean

A metric for quantitative assessment of modeled trajectories based on the two dimensional Kolmogorov-Smirnov statistical test is presented. The metric is used to show that ROMS model trajectories launched over the continental shelf throughout the SBC generally agree with observations with a few exceptions in specific regions.

Task 2: Wave-driven inner-shelf motions in Southern California

Drifting buoys that move onshore generally decelerate as they reached the surf zone. It is shown with model results that changes in the profiles of Stokes drift and undertow flow with water depth can give rise to enhanced offshore directed undertow flow, relative to

shoreward directed Stokes drift, of 2 cm/s over the depth of the drifter drogue (0.5 to 1.5 meters beneath the surface) that may explain the observed decelerations. Thus, during conditions of weak winds and strong wave forcing, the ability of a water parcel to cross the interface of the outer edge of the surf zone may have significant depth dependence.

Task 3: Circulation patterns over the inner-shelf of the Santa Barbara Channel

Circulation patterns over the inner-shelf of the Santa Barbara Channel cannot be mostly explained by a few coherent statistical modes or patterns, as is the case for currents further offshore. Thus, the circulation modes presented in Winant et al. (2003) are not necessarily applicable to the inner-shelf.

Study Products

Papers:

Ohlmann, J. C. and S. Mitarai, 2010. Lagrangian assessment of simulated surface current dispersion in the coastal ocean, *Geophys. Res. Lett.*, **37**, L17602, doi:10.1029/2010GL044436.

Ohlmann, J. C., M. R. Fewings, and C. Melton, Wave-driven currents just outside the surf zone in Southern California, *Journal of Physical Oceanography,* submitted manuscript in review.

Presentations:

Fewings, M.R., L. Washburn and J.C. Ohlmann, 2010. Flow patterns and connectivity on the inner shelf near Point Conception and around the Northern Channel Islands, California. Presented at 2010 Ocean Sciences conference, Portland, Oregon.

Executive Summary

Information Needed

The Santa Barbara Channel – Santa Maria Basin Coastal Circulation Study (SBC-SMB CCS), a large observational program aimed at improving the understanding and predictability of *large-scale* circulation patterns, focused on observations along the 100 m isobath and in deeper waters. A key result of the SBC-SMB CCS has been identification of the roles of local winds and a generally poleward pressure gradient in forcing surface currents, and the definition of characteristic circulation patterns for the Channel. Patterns were initially defined as "Upwelling", "Cyclonic", "Relaxation", "Propagating Cyclones", "Flood East" and Flood West" (Harms and Winant 1998), and later reduced to "Upwelling", "Surface Convergence" and "Relaxation" (Winant et al. 2003). The characteristic patterns are extremely important because they provide a simple model for the large-scale circulation in the SBC based on knowledge of currents at a few isolated (i.e. current meter) locations.

SBC-SMB data are from both current meter records and drifter tracks. Current meters were located throughout the SBC, but at depths of 100 m or greater (Harms and Winant 1998). Drifters were deployed at various locations and allowed to sample throughout the SBC. However, drifter data within ~2 km of the shore (i.e. over the inner continental shelf) were eliminated because they recorded relatively small velocities and might have even been beached (Dever et al. 1998). The ARGOS-CODE drifters used in the SBC-SMB study give position data with 1 km spatial accuracy every few hours and are not appropriate for resolving inner-shelf flow patterns. Thus, circulation patterns defined for the SBC hold only for basin-scale currents, and may not be indicative of flows over the inner-shelf. Dever et al. (1998) ultimately report that drifters over the inner-shelf "exhibited behavior quite different from drifters found in the open channel".

Information about flows over the inner-shelf, well inshore of the 100 m isobath is needed. The necessary information relates to questions such as: 1) What are the characteristic patterns of circulation over the inner-shelf? 2) How do the inner-shelf patterns relate to the basin-scale patterns reported by Winant et al. (2003)? 3) What are the dominant forcing mechanisms?

Research Summary

Task 1: Lagrangian Assessment of Simulated Surface Current Dispersion in the Coastal Ocean

A purely Lagrangian assessment of dispersion from modeled surface current trajectories in the coastal ocean is presented. Modeled trajectories come from ROMS simulations for the Southern California Bight during the 1996 through 1999 period. Data are from surface current trajectories collected primarily in the Santa Barbara Channel with CODE style drifters. Distributions of particle positions from trajectories emanating from launch locations within 10 kilometers of the coast throughout the Santa Barbara Channel that advect for one through four days (Lagrangian PDFs) are evaluated descriptively and quantitatively. The two dimensional Kolmogorov-Smirnov (K-S) statistical test for

comparing discrete sampled data with a known probability distribution is the quantitative basis. In general, dispersion distributions from observations are similar to Lagrangian PDFs computed from modeled trajectories and the K-S statistic quantifies this accordingly. A few specific regions of poor model-data agreement are indicated and discussed. The purely Lagrangian assessment, elucidates an improved understanding of model performance and ocean circulation beyond that offered in a Eulerian sense, and is necessary when modeled trajectories are utilized for applied oceanographic and marine ecology problems.

Task 2: Wave-driven inner-shelf motions in Southern California

Recent observational studies show wave-driven Eulerian offshore flow just beyond the surf zone, referred to as undertow, can be a significant component of the net cross-shore transport during periods of weak winds. This study explores the wave-driven undertow at two locations off the Southern California coast where shoreline, shelf, wind, and wave characteristics differ from those in previous studies. Both Eulerian and Lagrangian data are considered. Drifter observations show a consistent decrease in onshore velocity of 4 - 5 cm s^{-1} within a few hundred meters of the surf zone. Undertow is examined as an explanation for the observed Lagrangian decelerations. Eulerian velocities from bottom-mounted current profilers in water depths near 10 m, collected during times of light winds, are small (< ~1 cm s^{-1}), consistent with model predictions for weak wave forcing. However, model results suggest weakly forced undertow can decrease the velocity of shoreward-moving drifters by > 2 cm s^{-1} in shallower waters (< 8 m). During light wind conditions, undertow may even prevent onshore transport at specific depths just outside the surf zone. Adding predicted Stokes drift velocities to the Eulerian ADCP observations improves their agreement with coincident Lagrangian drifter observations.

Task 3: Circulation patterns over the inner-shelf of the Santa Barbara Channel

Time series of water velocity from Acoustic Doppler Current Profilers in ~15 m water depth and wind stress from NDBC buoys are used to describe the dominant inner-shelf flow patterns and their relation to local wind forcing. The velocity time series are 2-10 years long and cover 20 sites along the mainland north and south of Point Conception and around the Islands. The along-shelf flow on the mainland displays subtidal fluctuations that are coherent across most of the sites, suggesting strong along-shelf connectivity during poleward flow events. The cross-shelf circulation profiles form a surprisingly robust pattern, with important implications for larval transport. The mean profiles at 16 of the 20 sites have the same curved form, with the velocity more offshore at the surface and bottom than in the middle of the water column. This structure is similar to cross-shelf flow profiles found in the Middle Atlantic Bight and explained by a simple model with wind stress and pressure gradient forcing (Lentz, 2008). The remaining 4 sites, near headlands, have stronger, surface-intensified cross-shelf flow with a linear profile. The spatial and temporal complexity of the inner-shelf circulation around the Islands is underscored by empirical orthogonal function (EOF) analysis of the depth-average flow. Only one EOF out of 28 available is statistically unique, and it captures only 16% of the variance. This indicates the inner-shelf flow at the mainland and island sites as a whole is not well-organized or composed of only a few simple patterns. In contrast, EOF analysis

of mid- to outer-shelf flow yielded three statistically separate EOFs representing different surface flow states and capturing 50% of the variance (Harms and Winant, 1998).

Conclusions

The research shows that inner-shelf flows in the study area can be highly variable between sites. Modeled trajectories over the shelf generally agree with observations, however, they differ at a few specific locations. During periods of weak winds, often the case along the Santa Barbara coastline, wave forcing can influence the transport of passive tracers through the surf-zone interface. The research has thus provided new information about modeled surface current trajectory skill, spatial current coherence, and wave-driven flows over the inner-shelf, a region not considered in the SBC-SMB CCS.

Task 1:
Lagrangian Assessment of Simulated Surface Current Dispersion in the Coastal Ocean

Carter Ohlmann and Satoshi Mitarai

Abstract: A purely Lagrangian assessment of dispersion from modeled surface current trajectories in the coastal ocean is presented. Modeled trajectories come from ROMS simulations for the Southern California Bight during the 1996 through 1999 period. Data are from surface current trajectories collected primarily in the Santa Barbara Channel with CODE style drifters. Distributions of particle positions from trajectories emanating from launch locations within 10 kilometers of the coast throughout the Santa Barbara Channel that advect for one through four days (Lagrangian PDFs) are evaluated descriptively and quantitatively. The two dimensional Kolmogorov-Smirnov (K-S) statistical test for comparing discrete sampled data with a known probability distribution is the quantitative basis. In general, dispersion distributions from observations are similar to Lagrangian PDFs computed from modeled trajectories and the K-S statistic quantifies this accordingly. A few specific regions of poor model-data agreement are indicated and discussed. The purely Lagrangian assessment, elucidates an improved understanding of model performance and ocean circulation beyond that offered in a Eulerian sense, and is necessary when modeled trajectories are utilized for applied oceanographic and marine ecology problems.

1. Introduction

Regional coastal ocean observing systems exist in part to provide stakeholders with the best possible information for addressing a wide variety of applied coastal problems. Many applications are inherently Lagrangian, requiring trajectories to determine the "fate and transport" or "connectivity" of tracers. For example, coastal water quality management, ecosystem management, spill remediation, and search-and-rescue operations all require knowledge of dispersion from water parcel trajectories.

Lagrangian applications in the turbulent ocean require statistical approaches, and thus a large number of observations. Probability distributions of water parcel location as a function of initial position and advection time (hereafter "Lagrangian PDFs") are the required quantities. Direct observations with water following drifters are too sparse for computation of meaningful Lagrangian PDFs for more than a few combinations of initial position and advection time. Trajectories computed from numerical circulation models must therefore be relied on. In a recent study, *Mitarai et al.* [2009] determine Lagrangian PDFs with millions of trajectories computed from the Eulerian output of the *Dong and McWilliams* [2007] Southern California Regional Ocean Modeling System (ROMS) simulations. Results of *Mitarai et al.* [2009] are a part of the planning process for designation of Marine Protected Areas in Southern California.

Southern California ROMS simulations, the basis of the *Mitarai et al.* [2009] Lagrangian PDFs, compare favorably with observations in a Eulerian sense [*Dong et al.,* 2009]. Comparisons show agreement in the first two statistical moments and lead *Dong et al.* [2009] to conclude, "The model results resemble the observations in terms of the spatial structure and magnitude of the mean, interannual, seasonal, and intraseasonal variations". Eulerian agreement is not necessarily indicative of accuracy in trajectories, dispersion, or Lagrangian PDFs. Various Eulerian flow patterns can yield similar low order statistical moments, relatively small errors in Eulerian velocity statistics can become substantial when integrated and eddy structures can manifest themselves differently in Eulerian and Lagrangian frames [*Ohlmann and Niiler,* 2005].

This paper uses *in situ* drifting buoy data to assess dispersion distributions from modeled trajectories in a purely Lagrangian sense. Such an assessment is necessary prior to using modeled trajectories and their derived products in applied problems. The analysis gives a spatially continuous distribution of model skill that can elucidate an improved understanding of both model performance and ocean circulation beyond that offered in a Eulerian assessment. Limited densities of Lagrangian observations typically preclude such studies.

2. Data and Methods

2.1 ROMS Derived Trajectories

Results from the Southern California Bight ROMS simulations (SCB-ROMS), described in detail by *Dong and McWilliams* [2007] and *Dong et al.* [2009], are the basis for modeled trajectories. SCB-ROMS is a primitive equation hydrodynamic model with a free sea-surface, a horizontal curvilinear coordinate system, and a vertical sigma coordinate system [*Shchepetkin and McWilliams*, 2005]. The innermost of three nested grids has 1.0 km horizontal grid resolution. Model solutions are available for the 1996 through 2003 period.

Particle trajectories are computed from Eulerian velocity fields at 1 m depth using fourth order Adams-Bashford-Moulton predictor-corrector scheme with no sub-grid scale energy (hereafter "modeled trajectories"). The two-dimensional (2-D) velocity fields at 1 m are used for consistency with drifter observations. The 2-D modeled trajectories differ from the fully three-dimensional (3-D) trajectories described in *Mitarai et al.* [2009]. Fixed-depth tracking can lead to "beaching" compared with 3-D flows (particles that reach the shore in the surface layer continue their motion vertically in 3-D to satisfy continuity). Pathways of modeled trajectories are thus terminated when reaching a shoreline boundary just as *in situ* drifter observations terminate when they run ashore, or "beach".

Launch locations (located within 10 km of the coast), the scheme for launching modeled trajectories, and computation of Lagrangian PDFs from positions along surface current trajectories after some integration time, are all described in detail by *Mitarai et al.* [2009]. Lagrangian PDFs are computed for 1, 2, 3, and 4 day advection times allowing

trajectories to terminate through beaching. Nearly 200,000 trajectories launched from 1996 through 1999 and weighted by month and year to agree with the temporal distribution of observed trajectories (described below) are the basis of the Lagrangian PDF calculations.

2.2 Drifter Data

Two of the densest *in-situ* drifter studies performed to date are attributable to the United States Bureau of Ocean Energy Management, Regulation and Enforcement [BOEMRE; e.g. *Winant et al.,* 1999; *Winant et al.,* 2003; *Ohlmann and Niiler,* 2005]. Drifter data used here are a subset of those collected from May 1993 through November 1999 in the Santa Barbara Channel (SBC) and Santa Maria Basin (SMB) as part of the BOEMRE funded *Santa Barbara Channel – Santa Maria Basin Coastal Circulation Study*. Drifter design, deployment scheme, and resultant data, are all described in detail by *Dever et al.* [1998] and *Winant et al.* [1999, 2003]. Only observations from 1996 through 1999, the time period for which ROMS solutions are available, are considered here.

CODE design drifters are drogued at nominal depth near 1 m and follow water to within ~0.01% of the wind speed [*Davis,* 1985]. Up to six drifter positions per day are obtained via Doppler ranging with the satellite based Argos system. Position accuracy ranges from ~100 to 1000 m. Initially, single drifters were released roughly every two months from 12 stations located throughout the SBC [*Winant et al.*, 1999]. A dozen deployment locations in the SMB were added in May 1996. Deployment frequency decreased to near quarterly during the 1997 through 1999 period. Drifters have a nominal sampling life near 40 days. However, near half the drifters reportedly beached giving many short-lived tracks [*Dever et al*., 1998].

Since only starting and ending position data are required for this study, raw Argos position data are utilized. All drifter position records contained within each of the *Mitarai et al.* [2009] launch sites during the 1996 through 1999 period are first identified. For each individual drifter that passes through a launch site, the position record closest to the center time of all position records within the launch site is identified as the starting record. Ending positions after 1, 2, 3, and 4 days are identified by linearly interpolating between records. Drifter tracks without position records within +/- 8 hours of the ending time may have significant error in interpolated position and are thus eliminated. Drifter trajectories within 5 days of a previous launch are eliminated to insure independent observations.

2.3 Comparison Metric

The Kolmogorov-Smirnov (K-S) test is a non-parametric statistical method for determining if two distributions differ [*Press et al.,* 2002]. The test is based on the maximum difference in cumulative distribution functions (CDFs) of the distributions. It uses information from individual data points, can be used with relatively small sample sizes (as it does not require binning), can accept analytical PDFs, and can be applied to empirical distributions. These features make it attractive for comparing empirical PDFs with a limited number of drifter observations.

The K-S test has long been used with oceanographic data primarily to examine the Gaussianity of velocity distributions [e.g. *Swenson and Niiler,* 1996; *Bracco et al.,* 2000; *LaCasce*, 2005]. More recently, *van Sebille et al.* [2009] use the K-S test for binary determination of model skill with some confidence level. Lagrangian PDFs of modeled dispersion are not expected to be isotopic or spatially homogeneous as with Gaussian velocity distributions [*Mitarai et al*, 2009]. The focus here is on the K-S test statistic as a quantitative metric for assessing agreement in the spatial distribution of the ending positions of modeled and observed trajectories. Modeled dispersion is represented with analytical Lagrangian PDFs, and dispersion observations are represented as discrete positions.

The K-S test is based on the idea that different distribution functions, or data sets, give different CDFs, and the largest absolute difference in CDF values (D) is indicative of the probability of disagreement. The K-S test statistic (P)

$$P = 2\sum_{j=1}^{\infty}(-1)^{j-1}\exp\left(-2j^2\left[\frac{D\sqrt{N}}{1+\sqrt{1-r^2}\left(0.25-0.75/\sqrt{N}\right)}\right]^2\right) \quad (1)$$

described by *Press et al.* [2002] quantifies the confidence level associated with D. For application here, D is the maximum absolute difference between CDFs obtained from SCB-ROMS Lagrangian PDFs and drifter observations, N is the number of statistically independent drifter observations, and r is the correlation coefficient for zonal and meridional drifter positions determined in a least squares sense. D is determined as a function of launch location and advection time by considering probabilities in each of the four quadrants about all given drifter positions as described by *Fasano and Franceschini* [1987] and *Press et al*. [2002].

The K-S statistic is applied to cases with more than 10 independent drifter observations, a sufficiently large threshold for reliable use of the test statistic while allowing comparisons for the majority of the SBC. Histograms of 1000 random draws of various sample sizes between 10 and 20 agree with the analytical solution (Equation 1) when $P <$ ~0.2. Equation 1 degrades slightly with increasing sample size for P > ~0.2, however, the implication, that compared distributions are not significantly different, still holds [i.e. Press et al., 2002]. Dependence of the P statistic on values of N and r is discussed in detail by *Fasano and Franceschini* [1987] for $N = 5$ to 5000.

3. Results

A comparison of model Lagrangian PDFs and drifter observations is first indicated for a single arbitrarily selected launch site and four advection times to demonstrate the P value computation. Thirty *in situ* drifters emanate from the launch site during the model integration time. Positions of 17 independent drifters after 1, 2, 3, and 4 days of sampling are shown with corresponding Lagrangian PDFs (computed from positions of modeled trajectories weighted for temporal agreement with observations) in Figure 1 Lagrangian PDFs suggest primarily northwest movement towards the center of the SB Channel, and equator-ward movement around the east side of Santa Cruz Island. The PDFs show

spread throughout almost the entire SBC after 3 days, with the largest densities nearest the deployment location (Figure 1c).

The distribution of drifter positions after each of the four integration times is quantitatively compared with the corresponding model derived Lagrangian PDF through the *P* value (Equation 1). For each *in situ* drifter position (considering a specific integration time) the sample space is divided into four quadrants about that position as illustrated by dashed lines in Figure 1d. CDFs are then computed for each quadrant from the model Lagrangian PDF and drifter data as the integral of the modeled PDF and the relative number of drifter positions, respectively. *D* is computed as the maximum difference in model and observed CDFs considering the four sets (quadrants), and quantitative agreement between distributions is determined with *P* (Equation 1).

In situ drifter positions always exist where the model derived Lagrangian PDFs are non-zero for the advection times considered. Drifter positions after 1, 2, and 4 days show good qualitative agreement with Lagrangian PDFs, and $P \geq 0.08$ for these times (Figure 1a,b,d). After 3 days, the Lagrangian PDF has a pronounced southward extension that is matched by only a single drifter (Figure 1c). This discrepancy gives rise to a larger maximum difference in CDFs, and thus a much smaller *P* value ($P = 0.02$). These qualitative relationships for various values of *P* aid interpretation of the quantitative statistic.

Comparisons of modeled and observed dispersion distributions for six release sites and a 2 day advection time show qualitative relationships for a larger range of *P* values. For the launch site near Point Conception, both modeled and in situ distributions indicate similar movement mostly to the south with relatively large energy and this agreement is quantified with $P = 0.14$ (Figure 2a). Both modeled and observed trajectories that emanate from the north shore of San Miguel island are most likely to be transported either along the coast of Santa Rosa Island, toward the center of the SBC or equatorward around the east side of the island, and again the good agreement is quantified with a large *P* (0.77; Figure 2d).

Release sites with poor qualitative agreement have *P* values much less than the statistical threshold at the 95% confidence level. The majority of drifters released from the northwest tip of Santa Cruz Island end up to the northeast of the launch location after 2 days (Figure 2e). The PDF from modeled trajectories that emanate from this site has its greatest weighting directly south of the launch location where less than 20% of the drifters go ($P = 0.03$). Southward movement in model trajectories also differs from northeastward *in situ* drifter movement for the launch site on the north coast of Santa Cruz Island ($P = 0.02$; Figure 2f).

The cases shown in Figure 2 demonstrate major directional differences in observed and modeled trajectories when $P \leq 0.05$. Qualitatively good agreement exists in Figures 1 and 2 when $P > 0.05$. The spatial distribution of low *P* values, where modeled trajectories terminate in very different locations than observed, is relevant to the quest for improved model skill.

P values are computed for all defined launch sites and 1–4 day advection where > 10 independent drifter observations emanate, and all trajectories have ending positions within the ROMS domain. These constraints limit the advection times considered and explain why the set of launch sites resolved varies with advection time (Figure 3). The majority of launch site and advection time combinations considered give $P > 0.05$ indicating good agreement between ending distributions of modeled and observed trajectories. However, regions of poor agreement ($P \leq 0.05$) exist for launch sites in the northwest SBC for the 1-day advection time, and along the north coast of Santa Cruz and Santa Rosa Islands for all advection times (Figure 3).

Inconsistencies between simulated dispersal patterns and historical drifter data are not necessarily due to inaccuracies of the circulation simulations themselves. Some differences are expected given the 1 km resolution of ROMS, unresolved eddy energy known to exist [e.g. *Ohlmann et al.*, 2007], and the small size of Channel Island gaps. The ROMS trajectories do not include forcing from tides. Despite the fact that tidal flows in the SBC are mostly rectilinear with velocities < 5 cm/s, tidal energy in flows between Channel Islands can be significantly larger [*Munchow*, 1998] and this may explain low *P* values for launch locations near island gaps. The region of disagreement in the northwest SBC (Figure 3a) is characterized by large wind stress gradients that may not be adequately resolved in the ROMS simulations [e.g. *Dong et al.,* 2009]. The K-S test presented here allows the skill of future ROMS configurations (i.e. with tides and/or finer spatial resolution) to be quantitatively evaluated for most of the coastal domain in the SBC.

4. Conclusions and Summary

A purely Lagrangian validation of ROMS coastal dispersal simulations in the SBC region is presented. The Lagrangian assessment, believed to be the first of its kind, is a necessary step in understanding model skill and offers insight into model performance beyond traditional Eulerian comparisons. The assessment provides both quantitative and qualitative information regarding interpretation of model trajectory PDFs. “Fate and transport” type models that utilize simulated trajectories for applied problems should undergo this sort of Lagrangian assessment on their way to operational use.

The K-S test statistic *P* derives from the maximum difference in CDFs computed from model-based analytical PDFs and individual observations. The K-S test is appropriate for this application as it can be used with relatively small sample sizes, can accept analytical PDFs, and can be applied to empirical distributions. In addition to interpreting *P* in the usual binary statistical sense (accepting or rejecting a null hypothesis that the distributions differ), a more quantitative interpretation is used. Significant directional differences between modeled Lagrangian PDFs and observed drifter distributions exist when $P \leq 0.05$. Distributions show qualitatively good agreement when $P > 0.05$ as the binary statistic suggests.

The study focuses on ROMS derived trajectories that emanate from launch sites within 10 km of the coastline in the SBC from 1996 through 1999 and advect for up to 4 days.

The spatial domain over which comparisons are performed extends far beyond the more traditional Eulerian approach, typically confined to locations of a few scattered moorings. For the cases considered, ROMS-derived PDFs and in situ drifter observations do not, in general, differ substantially. The assessment indicates that observed and modeled Lagrangian distributions show consistently (among advection times) poor agreement in regions along the north coasts of Santa Cruz and Santa Rosa Islands, likely due to strong tidal flows through island gaps not resolved in simulations. Poor agreement in the northwest SBC for 1-day advection suggests a local, short-time mechanism. The K-S metric presented here enables a quantifiable Lagrangian skill assessment of future model configurations that attempt improved simulations.

References:

Bracco, A., J.H. LaCasce, and A. Provenzale (2000), Velocity PDFs for oceanic floats, *J. Phys. Oceanogr.,* 30, 461–474.

Davis, R.E. (1985), Drifter observations of coastal surface currents during CODE: The method and descriptive view, *J. Geophys. Res.*, *90*, 4741-4755.

Dever, E.P., M.C. Hendershott, and C.D. Winant (1998), Statistical aspects of surface drifter observations of circulation in the Santa Barbara Channel, *J. Geophys. Res.*, 103, 24,781–24,797.

Dong, C.M., and J.C. McWilliams (2007), A numerical study of island wakes in the Southern California Bight, *Cont. Shelf Res.*, 27(9), 1233–1248, doi: 10.1016/j.csr.2007.01.016.

Dong, C.M., E.Y. Idica, and J.C. McWilliams (2009), Circulation and Multiple-scale Variability in the Southern California Bight, *Prog. Oceanogr.,* 82(3), 168-190, doi: 10.1016/j.pocean.2009.07.005.

Fasano, G., and A. Franceschini (1987), A multidimensional of the Kolmogorov-Smirnov test, *Monthly Notices Royal Astronomy Society*, 225, 155-170.

LaCasce, J.H. (2005). On the Eulerian and Lagrangian velocity distributions in the North Atlantic. *J. Phys. Oceanogr*., 35(12), 2327–2336, doi: 10.1175/JPO2833.1.

Mitarai, S., D.A. Siegel, J.R. Watson, C. Dong and J.C. McWilliams (2009), Quantifying Connectivity in the Coastal Ocean, *J. Geophys. Res.*, 114, C10026, doi: 10.1029/2008JC005166.

Munchow, A. (1998), Tidal currents in a topographically complex channel, *Cont. Shelf Res.,* 18, 561-584.

Ohlmann, J.C., and P.P. Niiler (2005), Circulation over the continental shelf in the northern Gulf of Mexico, *Prog. Oceanogr.,* 64, 45-81, doi: 10.1016/j.pocean.2005.02.001.

Ohlmann, J.C., P.F. White, L. Washburn, E. Terrill, B. Emery, and M. Otero (2007), Interpretation of coastal HF radar derived surface currents with high resolution drifter data, *J. Atmos. Oceanic Technol.*, **24**, 666–680, doi: 10.1175/JTECH1998.1.

Peacock, J.A., (1983), Two-dimensional goodness-of-fit testing in astronomy, *Monthly Notices Royal Astronomy Society*, 202, 615-627.

Press, W.H., S.A. Teukolsky, W.T. Vetterling, and B.P. Flannery, (2002), *Numerical Recipes in C: The Art of Scientific Computing*, Cambridge University Press.

Shchepetkin, A.F., and J.C. McWilliams (2005), The regional oceanic modeling system (ROMS): a split-explicit, free-surface, topography-following-coordinate oceanic model, *Ocean Modelling*, 9(4), 347–404, doi: 10.1016/j.ocemod.2004.08.002.

Swenson, M.S., and P.P. Niiler (1996), Statistical analysis of the surface circulation of the California Current, *J. Geophys. Res.*, 101, 22,631–22,645.

van Sebille, E., P.J. van Leeuwen, A. Biastoch, C.N. Barron, and W.P.M. de Ruijter (2009), Lagrangian validation of numerical drifter trajectories using drifting buoys: Application to the Agulhas system, *Ocean Modelling,* 29, 269-276, doi: 10.1016/j.ocemod.2009.05.005.

Winant, C.D., D.J. Alden, E.P. Dever, K.A. Edwards, and M.C. Hendershott (1999), Near-surface trajectories off central and southern California, *J. Geophys. Res.*, 104, 15,713–15,726.

Winant, C.D., E.P. Dever, and M.C. Hendershott (2003), Characteristic patterns of shelf circulation at the boundary between central and southern California, *J. Geophys. Res.*, 108(2), 3021, doi:10.1029/2001JC001302.

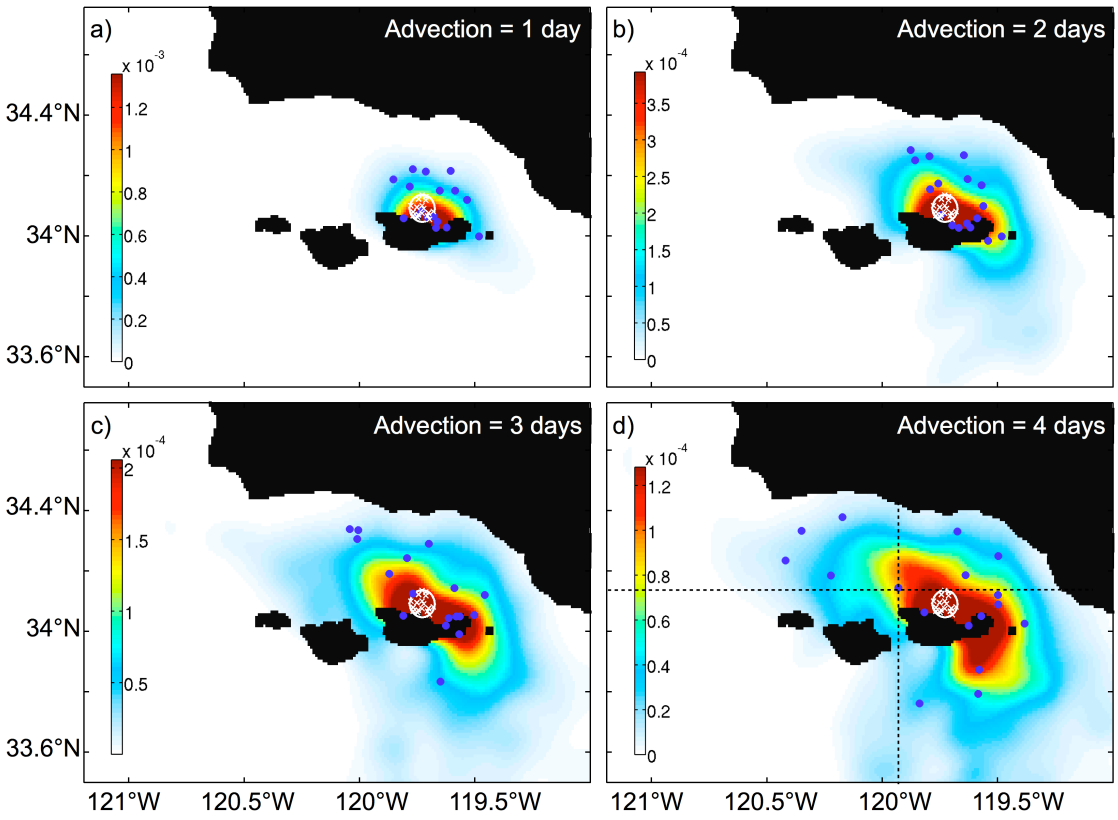

Figure 1. Lagrangian PDFs (color contours) from model output and locations of 17 surface drifters (blue dots) considering trajectories that emanate from a single launch site (white circle) for advection times of a) 1 day, b) 2 days, c) 3 days and d) 4 days. *P* values for the various advection times are a) 0.11, b) 0.12, c) 0.02 and d) 0.08. Dashed black lines in panel d, used to explain calculation of *P*, are discussed in the text. PDF units are km^{-2}.

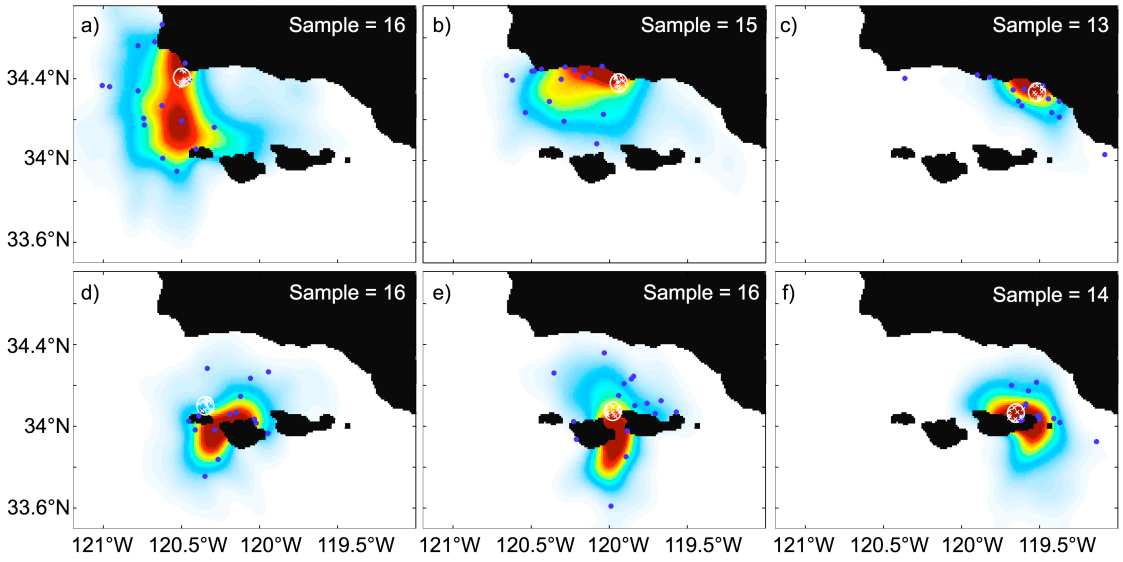

Figure 2. As in Figure 1 for selected launch sites (white circles) and an advection time of 2 days. *P* values for the various launch sites are a) 0.14, b) 0.05, c) 0.55, d) 0.77, e) 0.03 and f) 0.02. Sample size (n) for each comparison ranges from 13 to 16 and is indicated in the upper right of each panel.

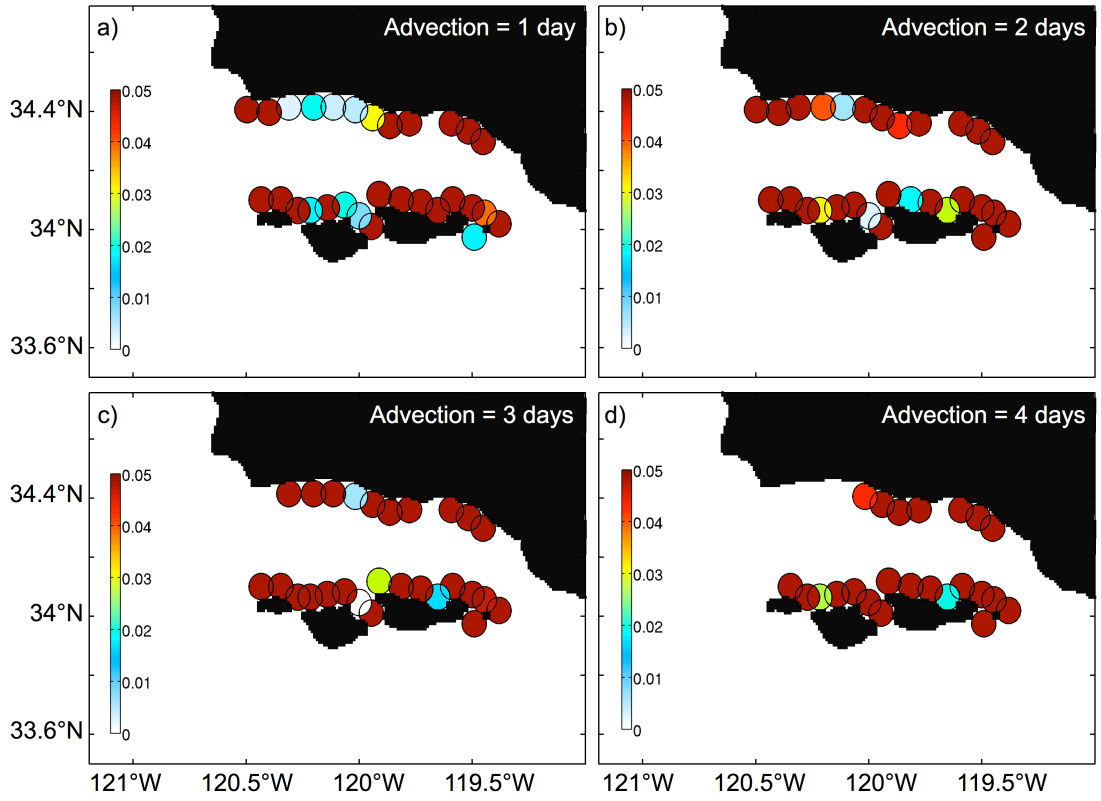

Figure 3. *P* values (colors) quantifying agreement between modeled and observed distributions of positions along trajectories for various coastal launch sites (locations of colored circles) and advection times of a) 1 day, b) 2 days, c) 3 days, and d) 4 days. Only cases with > 10 statistically independent drifter observations, and trajectories (observed and modeled) that remain within the model domain, are considered. Red sites ($P > 0.05$) indicate locations where observations are not distinctly unrepresentative of samples from corresponding model PDFs, at the 95% confidence level.

Task 2:
Wave-driven inner-shelf motions in Southern California

Carter Ohlmann and Melanie Fewings

1. Introduction

When surface gravity wave propagation is viewed in a reference frame rotating with the Earth, the Coriolis force destroys the exact quadrature between horizontal and vertical wave orbital velocities. This leads, in the wave-averaged momentum equation, to a Reynolds stress with vertical shear (Hasselmann, 1970). For a linear, steady state model with negligible turbulent mixing, the wave-driven shear stress generates (for an along-shore uniform domain) a mean Eulerian current that is exactly equal and opposite to the Stokes (1847) drift flow.

Observational studies of wave driven flow just seaward of the surf zone, referred to as undertow, are only recently appearing. Lentz et al. (2008) analyze moored profile data collected off the Massachusetts and North Carolina coasts, and find wave driven undertow to be the dominant component of the depth averaged cross-shelf flow (see also Fewings et al. 2008 for the combined effects of waves and wind). Both observed and modeled profiles have maximum velocities near the surface that decrease with depth. The shape differs from parabolic undertow profiles found in the surf zone where turbulent mixing is not negligible (e.g. Reniers et al. 2004). Kirincich et al. (2009) similarly investigate the wave driven undertow off the Oregon coast, characterized by a steep narrow shelf and a jagged coastline that contrast the Lentz et al. (2008) study site. Although the wave-driven flows observed off Oregon are similar to the Lentz et al. (2008) observations and model results, Kirincich et al. (2009) conclude that wave driven cross-shore processes off the Oregon coast are not significant when compared with local Ekman dynamics.

This study explores the wave driven undertow off the Southern California coast where shoreline, shelf, wind, and wave characteristics differ from those in the aforementioned studies. Santa Barbara lies almost directly east of Point Conception along a south-facing coastline such that direct effects of prevailing northwest winds and large swells from the North Pacific are limited (e.g. Brink and Muench, 1986, Winant et al. 2003). The northern Channel Islands are located ~40 km offshore and block nearly all swell from the southern hemisphere. The coastline is mostly jagged with largely sandy beaches, the shelf is steep and narrow, and waves are mostly short period with small amplitude. Huntington Beach, located between Los Angeles and San Diego, is characterized by a straight southwest-facing coastline and steep narrow shelf. During summer (Austral winter), HB receives direct impact from long-period, small-amplitude southern hemisphere swell (that can manifest in large breakers) and small amplitude, short-period wind waves.

Results are based on the analysis of coincidently sampled Eulerian and Lagrangian observations, an expansion of past studies. The Lagrangian drifter data show a consistent decrease in onshore velocity just outside of the surf zone. Cross-shore variations in undertow profiles are examined as an explanation for the observed Lagrangian

decelerations. Eulerian observations from a few bottom-mounted current profilers provide an inconclusive picture, as the measured wave driven undertow is mostly extremely small (< ~1 cm s^{-1}). However, the Lentz et al. (2008) model suggests undertow can significantly decrease the velocity of onshore moving drifters in the region shoreward of moored observations. Model results are consistent with observations at the mooring locations. Stokes drift, a Lagrangian phenomenon, is shown to rectify differences between the Eulerian and Lagrangian current observations.

2. Observations

Data are collected within ~1 km of the offshore edge of the surf zone in water depths ranging from ~2 to ~20 m, off the coasts of Santa Barbara and Huntington Beach, California (Figure 1; the study sites are subsequently refered to as "SB" and "HB", respectively). Eulerian velocity profiles and surface wave information are from bottom mounted upward looking acoustic Doppler current profilers (ADCPs) manufactured by RD Instruments (San Diego, CA). Santa Barbara data are from a single 600 kHz ADCP located ~0.5 km from the shoreline in a water depth of ~10 m that sampled from 18 November 2007 through 17 November 2008 (recovered quarterly to obtain data, and redeployed, resulting in a few missing days of data). Current vectors from the ADCP are averaged within 0.35 m bins every 4 minutes.

Huntington Beach velocity profiles are sampled as part of the HB06 experiment (e.g. Spydell et al. 2010) at four cross-shore locations in water depths of ~8 (2000 kHz), ~10 (1200 kHz), ~14 (600 kHz), and ~18 m (600 kHz) located ~0.6, ~1, ~2, and ~3 km from the shoreline, respectively. The mooring locations are subsequently referred to as "MG", "MF", "ME", and "MD", respectively. ADCP data at MG fail to adequately resolve the upper ~3 m of the water column, and are thus neglected. Average profiles are created in 1 m bins every 6 minutes with 600 kHz data, and for 0.5 m bins every 3 minutes with the 1200 kHz data. Data at MF and MD exist from July through October 2006, and data at ME extend from late September through October 2006. Significant wave height (H_{sig}), dominant wave period, and associated direction are determined with ADCP observations every 2 hours, through bursts of 2400 samples at a rate of 2 Hz (so surface wave frequencies are not aliased) and RD Instruments WavesMon v3.05 software. Huntington Beach wave data collected after 28 September 2006 appear suspect and are thus disregarded.

ADCP data are processed with bin locations defined relative to the time-varying ocean surface for determination of accurate near surface velocities. Tidal components are removed from ADCP data using T_TIDE (Pawlowicz et al. 2002), and the de-tided data are low pass filtered (1/36 hr^{-1}). Coordinate systems are defined such that the major and minor principal axes components of sub-tidal flow (u and v, respectively; major axis is in direction of greatest sub-tidal flow variance) align with the along- and cross-shore directions, respectively, and v is positive in the onshore direction.

Lagrangian observations are collected with Microstar drifters, drogued between ~0.5 and ~1.5 m beneath the surface, that sample their GPS position every 10 minutes. Microstar drifters follow horizontal motion of water to within ~0.1% of the wind speed (~1 cm s^{-1}

for 10 m s^{-1} winds). Details of drifter design, operation and water-following characteristics are given in Ohlmann et al. (2005). At Santa Barbara, 12 drifters are deployed roughly once each week (50 occurrences) during the ADCP sampling time. Considering occasional redeployments of drifters that quickly reached the surf zone, this gives a total of ~750 trajectories. At Huntington Beach, ~15 drifters are deployed on 15 days from 14 September trough 11 October 2006, resulting in a total of ~275 tracks considering redeployments. Drifter velocities are computed as a centered difference in position.

Spectral wave data from National Data Buoy Center (NDBC) buoys 46216 (located ~17 km southwest of SB) and 46230 (located ~2 km south-southwest of HB) are used to compute the Lagrangian Stokes velocity following

$$v_{st}(z) = \frac{H_{sig}^2 \omega k}{16} \frac{\cosh\left[2k(z+h)\right]}{\sinh^2(kh)} \cos(\theta_w) \quad (1)$$

where ω is wave frequency (rad s^{-1}), k is wavenumber (rad m^{-1}), θ_w is incident wave direction (relative to shore normal), h is water depth, and z is the vertical coordinate. Discussion of this formulation appears in Lentz et al. (2008) and Kirincich et al. (2009). The NDBC buoys measure wave energy and direction in nine continuous frequency bands. In Santa Barbara, $v_{st}(z)$ is computed with H_{sig} from ADCP observations, colored by normalized spectral energy coincidently observed at NDBC buoy 46216. Limited H_{sig} data from ADCPs in Huntington Beach requires that spectral wave data observed at NDBC buoy 46230 be propagated from the 22 meter isobath using conservation of wave energy. Directional relationships are determined spectrally at both locations to properly isolate the cross shore component. Given the interest in drifter decelerations, $v_{st}(z)$ is computed over the 0.5 to 1.5 m depth range, and subsequently indicated as v_{st}(1m).

Wind data are collected at the Santa Barbara airport, located ~18 km west of the Santa Barbara mooring, and at a moored buoy located ~2 km directly offshore of MD at Huntington Beach. To isolate wave driven flow, only data collected during periods of low winds (wind stress $\tau < 0.05$ N m^{-2}) are presented. This "low wind" threshold gives similar results, but with more data, compared with $\tau < 0.03$ N m^{-2} used by Lentz et al. (2008) and Kirincich et al. (2009).

To further isolate surface wave forcing (the focus of this study), Eulerian observations during low wind, large wave conditions are examined relative to the mean flow during low wind, small wave conditions. Small and large wave regimes are defined using H_{sig} and v_{st}(1m) criteria at SB and HB, respectively. Poorly resolved spectral wave data (due to the relatively distant location of buoy 46216) and little long-period swell at the Santa Barbara site make H_{sig} criteria preferable. The close proximity of spectral wave data and the contribution of long period swell (with little influence on v_{st}(z)) to H_{sig} at Huntington Beach make the v_{st}(1m) criteria preferable. Mean values of H_{sig} and v_{st}(1m) for the low

wind period, defined as $\overline{H_{sig}}$ and $\overline{v_{st}(1m)}$, and their associated standard deviations, defined as σ_{Hsig} and σ_{vst}, are computed at each of the sites. Mean small wave quantities are computed from observations at Santa Barbara (Huntington Beach) during times when $H_{sig} < (\overline{H_{sig}} - 0.5\sigma_{Hsig})$ $(v_{st}(1m) < (\overline{v_{st}(1m)} - 0.5\sigma_{vst}))$, and mean large wave quantities are computed from observations when $H_{sig} > (\overline{H_{sig}} + 0.5\sigma_{Hsig})$ $(v_{st}(1m) > (\overline{v_{st}(1m)} + 0.5\sigma_{vst}))$. The aforementioned statistics are given in Table 1. The small change in $\overline{H_{sig}}$ between the small and large wave cases at Huntington Beach (0.23 m), relative the near tripling in $\overline{v_{st}(1m)}$ (0.37 to 1.02 cm s^{-1}), demonstrates motivation for the site specific data filters.

3. Results

3.1 Drifter Decelerations

Consistent deceleration in the onshore velocity of drifters approaching the surf zone during low wind conditions is the most interesting observational result. For drifters deployed in Santa Barbara that move into waters shallower than 5 m, the onshore velocity component is mostly constant, between ~2 and 12 cm s^{-1}, between the ~12 and 5 m isobaths (Figure 2a). Once drifters reach water shallower than ~4 or 5 m, their onshore velocities consistently decrease. Onshore velocities inshore of the 3 m isobath are always < ~5 cm s^{-1}. The average velocity decreases from ~6 cm s^{-1} offshore of the 5 meter isobaths to ~2 cm s^{-1} at the 3 meter isobath, a cross shore distance of ~100 meters.
The observed deceleration at Huntington Beach occurs in deeper water, and the depth at which deceleration begins is more variable than in Santa Barbara. These results likely reflect the elevated and more variable wave energy in Huntington Beach that manifest in a surf zone with a deeper outer edge, and an outer edge with greater depth variability. For drifters deployed in Huntington Beach that move onshore of the 10 m isobath during low winds, the onshore velocity component varies between ~15 and 5 cm s^{-1} (Figure 2b). The average velocity gradually decreases from ~6 cm s^{-1} at the 12 m isobath, to < ~3 cm s^{-1} inshore of the 10 m isobath. Average values inshore of the 8 meter isobath are similarly < ~3 cm s^{-1}, but come from a reduced number of observations collected during periods of a narrower surf zone. Velocities less than zero (i.e. they reverse direction and move offshore) routinely occur.

3.2 Wave Driven Flow

Observed mean wave driven undertow flow profiles are computed by subtracting the mean low wind, small wave profiles from the mean low wind, large wave profiles. The mean undertow in Santa Barbara is 0.7 ± 1 cm s^{-1} in the topmost ADCP bin considered (~2 m depth), and decreases somewhat linearly with depth to ~0 ± 1 cm s^{-1} just above the bottom (Figure 3a). In Huntington Beach, the mean observed undertow profile also shows a velocity near 0.7 ± 1cm s^{-1} in the topmost ADCP bin considered (~2 m), that decreases with depth to ~0 ± 1 cm s^{-1} at ~ 6 m depth and beyond (Figure 3b).
Mean theoretical undertow profiles computed using the Lentz et al. (2008) model, forced with the same spectral wave data used to compute $v_{st}(z)$ during the low wind and large wave regime, are in good qualitative agreement with observations (Figure 3). In Santa Barbara, the mean modeled undertow velocity at 2 m is ~0.7 cm s^{-1}, nearly the same as

observed. In Huntington Beach, the modeled value is slightly larger than observed. The correlation coefficient (computed from linear least squares) between the depth averaged cross shore undertow flow from observations and the Lentz et al (2008) model is 0.67 in Santa Barbara. A statistically significant relationship does not exist in Huntington Beach where observations span a narrow range, compared with Santa Barbara.

3.3 Eulerian and Lagrangian Velocity Comparisons

Drifter velocities and coincidently sampled 20 minute average ADCP velocities are compared to determine if measurement differences can be rectified by subtracting $v_{st}(1m)$ from Lagrangian drifter observations. Comparisons are made with average velocity over the top three bins of ADCP data collected at Santa Barbara (DEPTH RANGE) and MF (Huntington Beach; DEPTH RANGE) when drifters are within 200 and 400 m of the moorings, respectively. SAY WHY DEPTH AVERAGING Beyond these distances, correlation coefficients decrease dramatically. Comparisons are made with 250 drifter velocites from 42 different days at Santa Barbara, and with 95 drifter velocites from 13 different days at Huntington Beach.

Root mean square (rms) velocity differences for along- and cross-shore components at both Santa Barbara and Huntington Beach are between 3.2 and 3.3 cm s^{-1} (Figure 4). Mean differences, however, are near 0.75 cm s^{-1} in the alongshore direction, but > 2.0 cm s^{-1} in the cross-shore direction, with drifters recording greater onshore and downcoast (equatorward) flow as expected. Spatial inhomogeneity, difference in sampling depth, and non-normal wave incidence likely explain the ~0.75 cm s^{-1} difference that exists in both velocity components. Polarity at both locations suggests drifter observations give $v_{st}(1m)$ = ~1.25 cm s^{-1} that is not resolved in ADCP measurements. When ADCP velocities are extrapolated to the drifter sampling depth, mean differences at Huntington Beach decrease by ~0.3 and 0.6 cm s^{-1} in the along- and cross-shore directions, respectively (mean differences at Santa Barbara are nearly unchanged). Cross-shore velocity differences, beyond those in the along-shore direction, are consistent with the magnitude of both $v_{st}(1m)$ and undertow velocities determined from observations, as described below.

The difference between the Eulerian (ADCP) and Lagrangian (drifter) velocities is a strong function of direction (Figure 5). Maximum differences generally align with the direction of $v_{st}(1m)$, and directions of maximum difference are almost exactly orthogonal to directions of 0 mean difference. At Santa Barbara, $v_{st}(1m)$ is primarily from southwest (~25 to 45°) of shore normal. Directions of maximum rms (3.61 cm s^{-1}) and mean (2.53 cm s^{-1}) velocity differences are 45 and 20°, respectively. At Huntington Beach, $v_{st}(1m)$ is from a larger range of angles (~5 to 50° southwest of shore normal) that similarly aligns with directions of maximum rms (3.43 cm s^{-1} from 45°) and mean (2.13 cm s^{-1} from 45°) velocitiy differences. Mean differences at Santa Barbara and Huntington Beach decrease by up to ~0.50 and 0.65 cm s^{-1}, respectively, in the expected directions, when $v_{st}(1m)$ is added to the ADCP velocities (black and grey dots in Figure 5).

4. Discussion

Observed wave forcing just outside the surf zone at Santa Barbara and Huntington Beach is weaker than reported by Lentz et al. (2008) and Kirincich et al. (2009) for the Oregon,

Massachusetts, and North Carolina coasts (for the chosen sampling periods). Background (low wind and small wave) velocity profiles removed to isolate wave driven flow are computed by Lentz et al. (2008) and Kirincich et al. (2009) as averages during times when $H_{sig} < 0.75$ m and 0.70 m, respectively. The Santa Barbara observations are characterized by $\overline{H_{sig}} = 0.81$ m during the *large* wave regime, and the background flow profile removed is computed for times of $H_{sig} < 0.38$ m (Table 1). The smaller undertow velocities observed at Santa Barbara are commensurate with weaker wave forcing.
The average undertow during the low wind and small wave regime at Huntington Beach is *greater* than that during the low wind and large wave regime, when wave regime is defined with H_{sig} criteria (as for Santa Barbara). Long period southern hemisphere swell of varying amplitude often contributes to H_{sig} at Huntington Beach. Such waves are characterized by large phase speed, c, and undertow is proportional to c^{-1} (for constant H_{sig}/h). Thus, use of $v_{st}(1m)$ for defining wave regimes at Huntington Beach. Despite $\overline{H_{sig}} = 0.72$ during the low wind and small regime (defined with $v_{st}(1m)$), background flow removed is much smaller than in previous studies. The Lentz et al. (2008) model accurately represents the observed undertow for smaller H_{sig} than previously examined. It is, however, important that the correct amplitude is given for steep, short period waves that have the greatest contribution to $v_{st}(z)$, and thus undertow. While the observed undertow (< ~1 cm s^{-1}) is undoubtedly small, that is the case at two discrete locations. Understanding the influence of wave forcing on observed drifter decelerations requires $v_{st}(1m)$ and associated undertow between 0.5 and 1.5 m depth to be considered for a range of h. Mean values of observed wave spectra during the large wave regime are used to compute $v_{st}(1m)$ and force the Lentz et al. (2008) model for $h <$ ~15 m at both Santa Barbara and Huntington Beach using a constant sloping bottom and realistic bathymetry. For $h >$ ~5 and ~6 m at Santa Barbara and Huntington Beach (considering realistic bathymetry), respectively, $v_{st}(1m)$ and its resultant undertow combine for no net cross-shore wave driven flow within the 0.5 to 1.5 m depth range (Figure 6). When h shoals to ~5 m at Santa Barbara, the undertow magnitude overcomes $v_{st}(1m)$, resulting in a net offshore velocity that increases to ~2 cm s^{-1} as h decreases to ~3 m. The mean observed onshore drifter velocity at Santa Barbara decreases by ~3 cm s^{-1} between h = 5 and 3 m (Figure 2). The velocity change is sensitive to cross-shore variations in bathymetry and to the location where the eddy viscosity specified in the model increases to represent the surf zone. The Lentz et al. (2008) model results thus suggest the transition of the wave driven undertow profile from a Hasselmann profile offshore to a parabolic profile near the surfzone can play a primary role in forcing observed drifter decelerations at Santa Barbara.

At Huntington Beach, the Lentz et al. (2008) model indicates undertow magnitude overcomes u_s when h shoals to ~6 m, and the modeled deceleration is much more abrupt (for realistic bathymetry) than at Santa Barbara. Modeled offshore velocity at Huntington Beach increases from near -1 to ~2 cm s^{-1} as h decreases from ~6 to ~3 m (Figure 6). However, the mean observed onshore drifter velocity decelerates as h shoals from ~13 to ~8 m, much deeper than the model indicates (Figure 2). Long period southern hemisphere swell, with relatively small amplitude, resulted in large breakers making for a surf zone that is much wider than the model predicts. Mean observed velocities decrease from ~10 to ~2 cm s^{-1}, much larger than the model shows. Transient rip currents, routinely

observed at Huntington Beach, likely explain occasional flow reversals observed just beyond the surf zone, and perhaps contribute to decelerations (Figure 2).

5. Conclusions and Summary

Recent studies suggest the Hasselmann (1970) wave driven undertow flow can be a significant part of the cross-shore momentum budget just beyond the surf zone, when examined in a Eulerian sense (Lentz et al. 2008, Kirincich et al. 2009). This study explores the undertow flow in Southern California (a region with wave, shelf, and shoreline characteristics that differ from those of past studies) with both Eulerian and Lagrangian observations. Mean observed Eulerian undertow flows for the time period characterized by little wind and the strongest wave forcing are < 1 cm s^{-1}. Velocities reach ~2 cm s^{-1} near the surface during the largest wave event observed. Small undertow velocities reflect small wave forcing compared with past studies, and agree with predicted undertow magnitudes.

Lagrangian observations give the more interesting results. The mean velocity of shoreward moving drifters during times of weak wind and strong wave forcing decreases by between 4 and 8 cm s^{-1} just beyond the outer edge of the surf zone at two Southern California locations. The Lentz et al. (2008) model suggests the depth dependent wave driven undertow explains ~3 cm s^{-1} of the observed decelerations. The increased undertow in the model comes from changes in the depth dependent flow that arise from changes in h through H_{sig}/h, and increased eddy viscosity approaching the surf zone. During periods of relatively weak net (depth integrated) onshore transport, as is often the case in Southern California, the wave driven undertow flow may retard, or even prevent, onshore flow at specific depths. The new Lagrangian observations add strength to the final conclusion in Lentz et al. (2008), that cross-shore transport to/from the surf zone, important for a variety of applied problems, is not fully understood.

References

Brink, K. H., and R. D. Muench, 1986. Circulation in the Point Conception - Santa Barbara Channel Region. *Journal of Geophysical Research*, **91**(C1), 877-895.

Fewings, M., S. J. Lentz, and J. Fredericks, 2008: Observations of cross-shelf flow driven by cross-shelf winds on the inner continental shelf. *J. Phys. Oceanogr.*, **38**:2358–2378, doi:10.1175/2008JPO3990.1

Hasselmann, K., 1970: Wave-driven inertial oscillations. *Geophys. Fluid Dyn.*, **1**:463–502.

Kirincich, A. R., S. J. Lentz, and J. A. Barth, 2009: Wave-Driven Inner-Shelf Motions on the Oregon Coast. Journal of Physical Oceanography, 39, 2942-2956, doi:10.1175/2009JPO4041.1

Lentz, S. J., M. Fewings, P. Howd, J. Fredericks, and K. Hathaway, 2008: Observations and a model of undertow over the inner continental shelf. *J. Phys. Oceanogr.*, **38**:2341–2357, doi:10.1175/2008JPO3986.1

Ohlmann, J. C., P. F White, A. L. Sybrandy, and P. P. Niiler, 2005: GPS-cellular drifter technology for coastal ocean observing systems, *Journal of Atmospheric and Oceanic Technology*, **22**, 1381-1388.

Pawlowicz, R., R. C. Beardsley, and S. J. Lentz, 2002: Harmonic analysis including error estimates in MATLAB using T TIDE. *Computers and Geosciences*

Reniers, A. J. H. M., E. B. Thornton, T. P. Stanton, and J. A. Roelvink, 2004: Vertical flow structure during Sandy Duck: Observations and modeling. *Coastal Eng.*, **51**:237–260.

Spydell, M., F. Feddersen, and R.T. Guza, 2009: Observations of drifter dispersion in the surfzone: The effect of sheared alongshore currents. *J. Geophys. Res. Oceans*, 114, C07028, doi:10.1029/2009JC005328.

Stokes, G. G., 1847: On the theory of oscillatory waves. *Trans. Cambridge Philos. Soc.*, **8**:441–455.

Winant, C. D., E. P. Dever, and M. C. Hendershott (2003), Characteristic patterns of shelf circulation at the boundary between central and southern California, *J. Geophys. Res.*, *108*(C2), 3021, doi:10.1029/2001JC001302.

site	low wind	low wind, small waves	low wind, large waves
SB	$\overline{H_{sig}}$ = 0.54 ± 0.33 m $\overline{v_{st}(1m)}$=0.45±0.28 cm s^{-1} n = 357 days	$\overline{H_{sig\text{-}sw}}$ = 0.41 ± 0.06 m $\overline{v_{st\text{-}sw}(1m)}$=0.27±0.11 cm s^{-1} n = 105 days	$\overline{H_{sig\text{-}lw}}$ = 0.81 ± 0.27 m $\overline{v_{st\text{-}lw}(1m)}$=0.79±0.45 cm s^{-1} n = 46 days
HB	$\overline{H_{sig}}$ = 0.82 ± 0.17 m $\overline{v_{st}(1m)}$=0.63±0.28 cm s^{-1} n = 99 days	$\overline{H_{sig\text{-}sw}}$ = 0.72 ± 0.17 m $\overline{v_{st\text{-}sw}(1m)}$=0.37±0.09 cm s^{-1} n = 36 days	$\overline{H_{sig\text{-}lw}}$ = 0.95 ± 0.14 m $\overline{v_{st\text{-}lw}(1m)}$=1.02±0.20 cm s^{-1} n = 26 days

Table 1. Significant wave height and undertow statistics by site (rows) during periods of low winds (column1), low winds and small waves (column 2), and low winds and large waves (column 3). Means, standard deviations and sample size (n) are indicated. Quantitative definitions for the 3 regimes are given in the text. Undertow values at an indicated depth of "1 m" are depth averaged between 0.5 and 1.5 m beneath the sea surface.

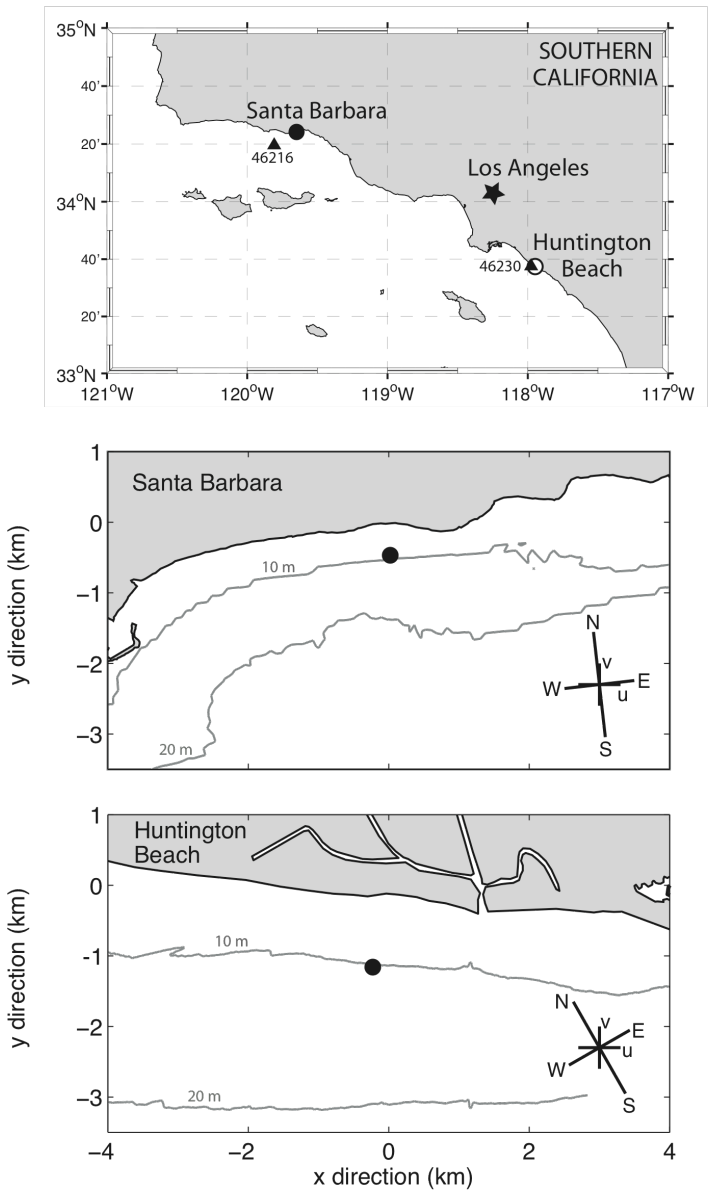

Figure 1. Mooring locations at the Santa Barbara (SB) and Huntington Beach (HB) sites, located along the Southern California coast. Bathymetry contours are shown at 10 and 20 meters. Location of NDBC moorings are shown with triangles. Principle axis coordinate system rotations are shown.

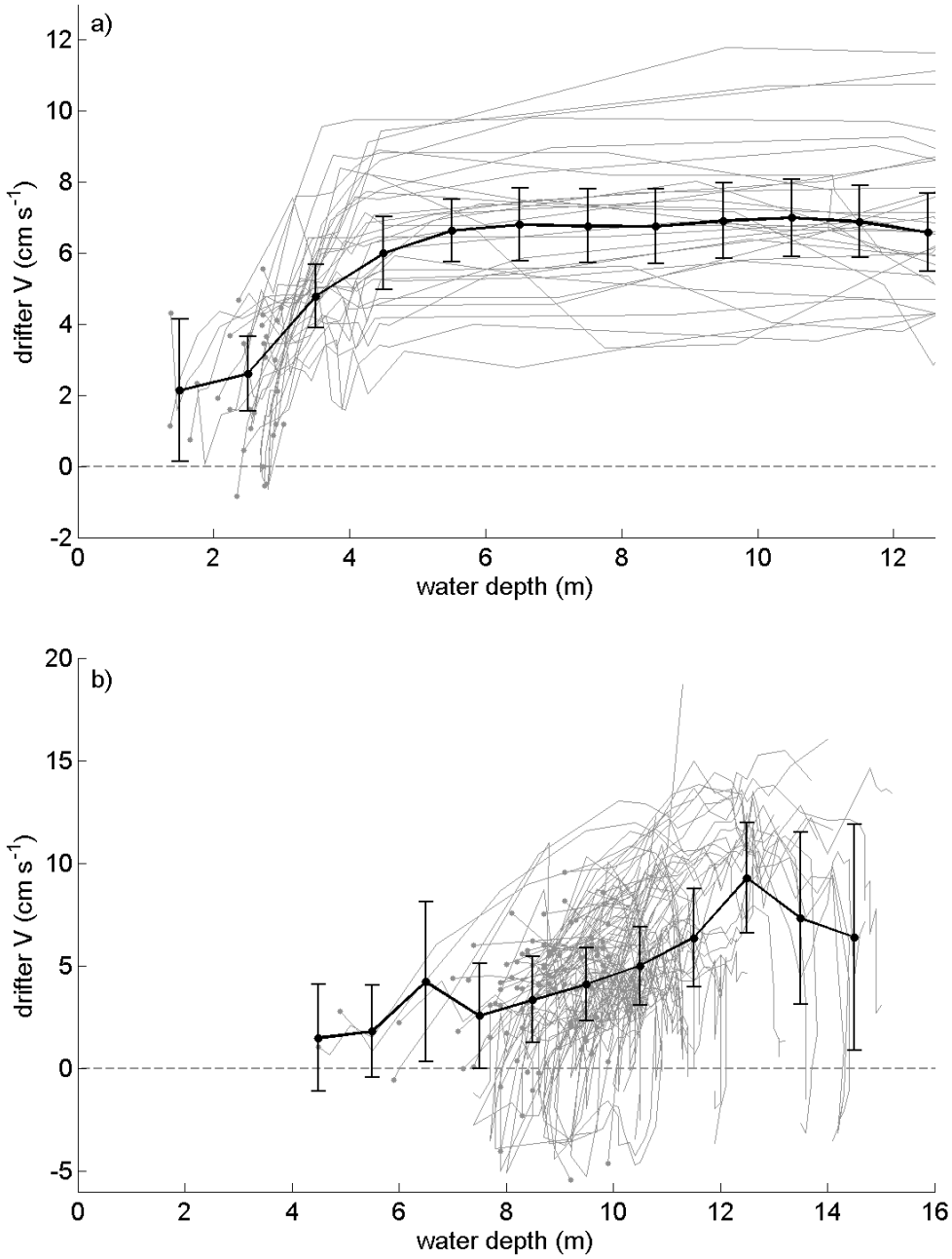

Figure 2. Onshore component of drifter velocity versus water depth, during low wind conditions, for all drifters that move shoreward of the a) 5 meter isobath at Santa Barbara, and b) 10 meter isobath at Huntington Beach. Last positions recorded by drifters prior to recovery are indicated with grey dots. Means of onshore velocities interpolated to the locations of integer bathymetry values are shown with black dots and connected with black lines.

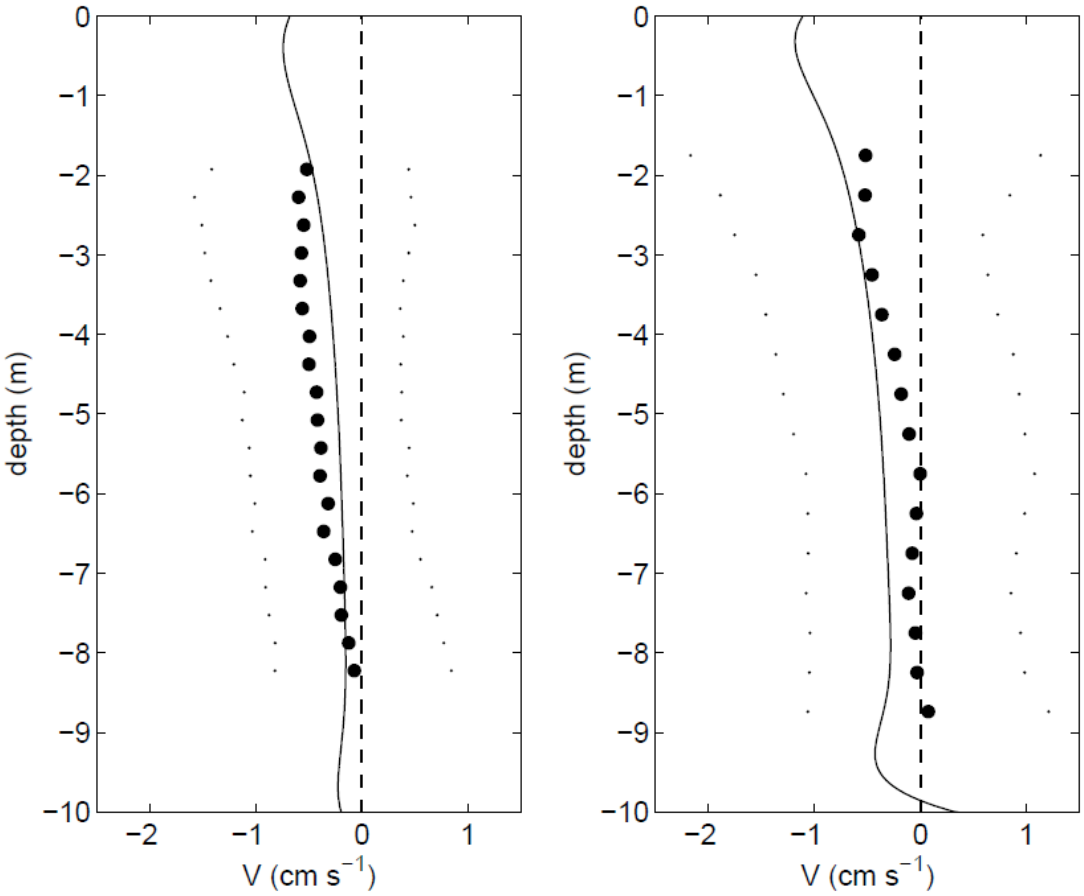

Figure 3. Mean Hasselmann (1970) flow profiles computed from ADCP data (black dots) collected at a) Santa Barbara and b) Huntington Beach. Grey dots indicate ± 1 standard deviation. Thin solid line: corresponding mean profile from Lentz et al. (2008) model forced with observed wave characteristics during times of observations.

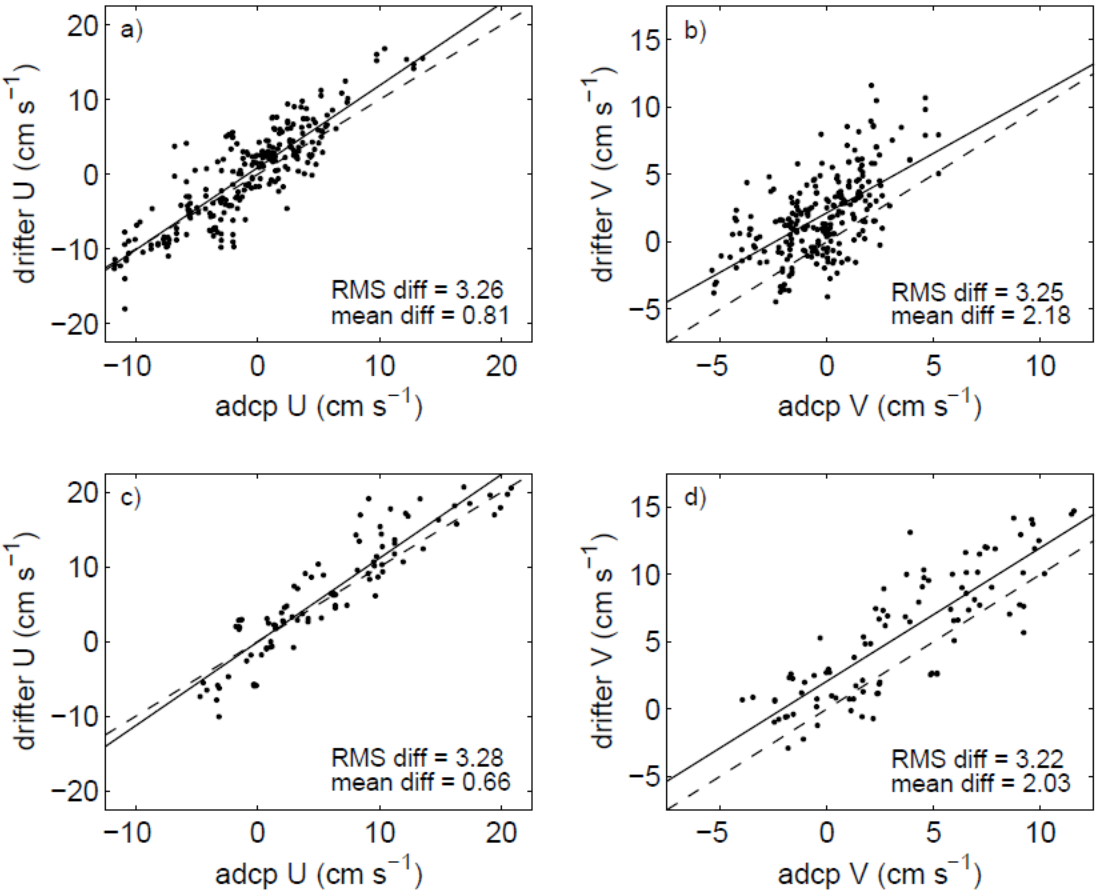

Figure 4. Coincidently sampled Eulerian and Lagrangian along-shore (a,c) and cross-shore (b,d) average velocities for each drifter that sampled within 200 meters of the SB ADCP (a,b), and 400 meters of the HB ADCP (c,d). Solid and dotted lines give best (least squares) fit and 1:1 lines, respectively. Drifter drogues extend from 0.5 to 1.5 meters depth. ADCP velocities are averages over the top 3 available bins, which extend from 1.9 to 2.6 and 1.8 to 2.8 m depth at the SB and HB moorings, respectively.

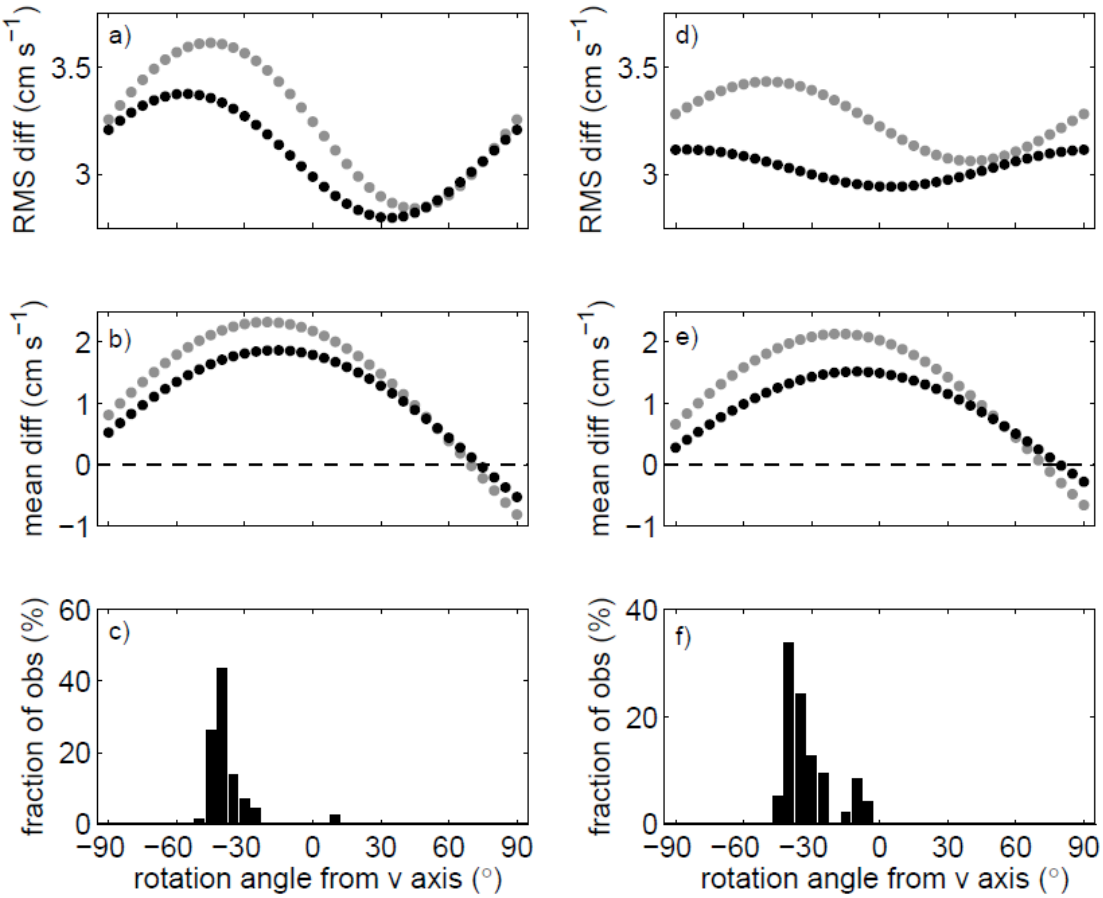

Figure 5. Differences between coincidently sampled Eulerian and Lagrangian velocities (shown in Figure 4) as a function of direction with (gray dots) and without (black dots) adding predicted Stokes drift to the ADCP velocities. Left and right panels give data from SB and HB, respectively. Top and middle rows give rms and mean difference values, respectively. Distributions of Stokes drift directions are given in the bottom panels, with 0° being shore-normal and negative angles indicating waves from a more up-coast (poleward) direction.

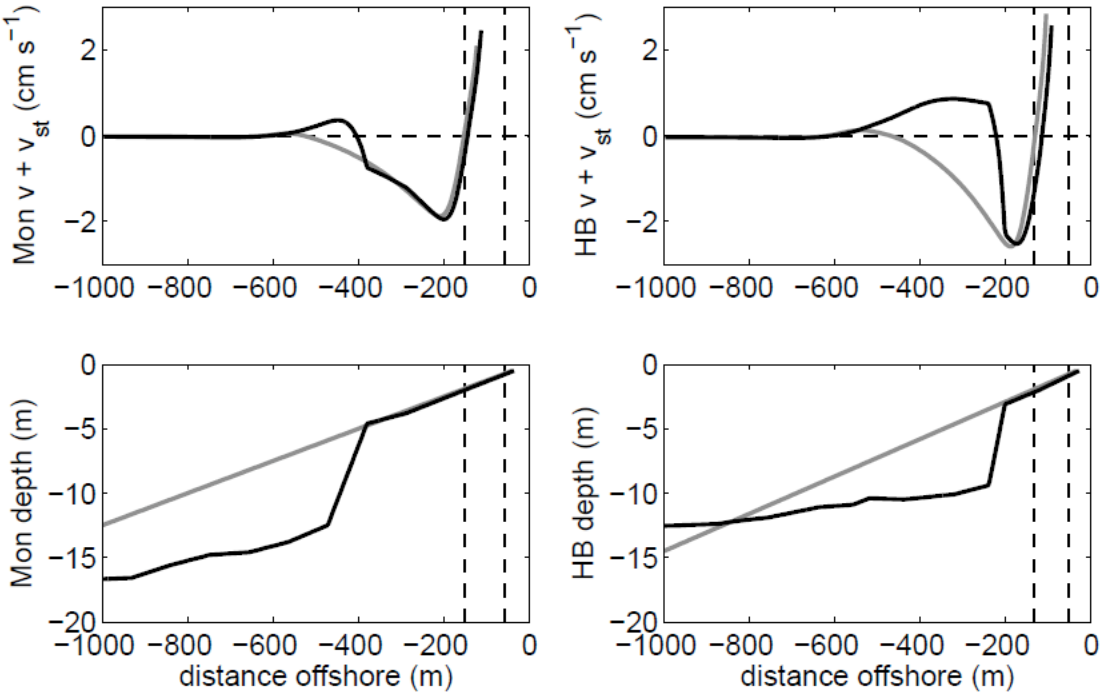

Figure 6. Sum of u_s and predicted undertow flow averaged over the 0.5 to 1.5 meter depth range for Santa Barbara (top left) and Huntington Beach (top right). Undertow velocity is computed with the Lentz et al. (2008) model forced with observed mean large wave conditions, using realistic bathymetry (black curves) and a constant sloping bottom (grey curves). Water depth as a function of offshore distance for Santa Barbara (left) and Huntington Beach (right) is shown in the bottom panels. Vertical dashed lines represent an estimated range for the outer edge of the surf zone.

Task 3:
Circulation patterns over the inner-shelf of the Santa Barbara Channel

Carter Ohlmann and Melanie Fewings

1. Introduction

The regional circulation in the Santa Barbara Channel (SBC), beyond the inner shelf, is relatively well studied. The southward-flowing California Current separates from the mainland near Point Conception (Checkley and Barth, 2009). Three circulation patterns, accounting for ~50% of the observed velocity variance in the SBC, are described by Winant et al. (2003). However, the circulation patterns in the central SBC are not necessarily indicative of the inner shelf circulation. For example, wind stress in the area southeast of Point Conception, in the "upwelling shadow" or lee of the bend in the coastline, is much weaker than further offshore, and is expected to drive different circulation patterns near the shore.

Over the past 10 years, current profiles have been recorded at 21 sites in 10-18 m water depth along the mainland coast and at the Islands (Figure 1). These data are used to describe a variety of flow states that exist over the inner shelf region, that are not necessarily correlated to the Winant et al. (2003) SBC scale flow patterns. The moored observations provide a much longer time record than can be obtained with the release of drifting buoys as originally proposed.

2. Data

The water velocity data were collected by the Partnership for Interdisciplinary Studies of Coastal Oceans (PISCO), the Santa Barbara Coastal Long-Term Ecological Research project (SBC- LTER) and the Channel Islands National Marine Sanctuary (CINMS) during 1999-2009. Water velocity was measured at 21 sites in 15-18 m water depth every 1 m from 2.5 meters above bottom (mab) to about 3 m below the mean water surface using bottom-mounted acoustic Doppler current profilers (ADCPs), except at two SBC-LTER sites on the mainland, CAR and MKO, where the water depths are 8 and 10 m and the velocity was measured every 0.5 m from 1.5 mab to 1.5 m below the surface. Water velocity was recorded as 2-min averages, low-pass filtered with a 1-hr moving window, and interpolated onto a common 20-min time base to form the ``high-frequency'' data set. ADCP bin depths were determined based on transducer height (mab) and position of the signal beam intensity maximum denoting the water surface. Data from ADCP bins within ~15% of the water depth below the surface are contaminated by side-lobe reflections and were discarded, based on abrupt changes in the ADCP signal percent good and the tidal velocity and phase profiles computed with the T_TIDE Matlab package (Pawlowicz et al., 2002). Each 20-min average velocity profile in which at least 75% of the bins contained good data was linearly interpolated in the vertical direction to fill holes in the profile that are assumed to be from fish or drift kelp blocking the beams. Wind velocity and air pressure data are from 6 National Data Buoy Center (NDBC) buoys

(http://www.ndbc.noaa.gov), 9 mainland coastal meteorological stations (mainly airports), and 4 island-based meteorological stations. Sea level data are from coastal tide gauges maintained by the National Oceanic and Atmospheric Administration (http://tidesandcurrents.noaa.gov) at Port San Luis, Santa Barbara, and Santa Monica.

To calculate wind stress τs, the drag law of Smith [1988] was used. To calculate depth-average velocities, data from the top and bottom good ADCP bins were extrapolated to the surface and bottom of the water column assuming a constant velocity near-surface and near-bottom, and then a trapezoidal estimate of the vertical integral was computed. In order to focus on time scales of days and longer, tides and other high-frequency motions were removed by detiding the velocities with T_TIDE [Pawlowicz et al., 2002], filling gaps < 24 hr in all time series by linear interpolation, and low-pass filtering with a $(33\ hr)^{-1}$ half-amplitude cutoff. The low-pass-filtered velocity observations are subsequently referred to as subtidal flow. Velocity and wind stress at each location are transformed into local along-shelf/cross-shelf coordinate systems based on the principal axes of the low-pass filtered wind stress or depth-average flow, with the major principal axis defining the along-shelf direction (Figures 2 and 3). The along-shelf flow is v, positive west- or northward, and the cross-shelf flow is u, positive north- or eastward. The symbols uda, and vda are used to indicate depth-average velocity components. Along-shelf pressure differences were estimated from the coastal tide gauge data with synthetic subsurface pressure (SSP) constructed similarly to Harms and Winant [1998]. This method takes into account the effects of both sea level and atmospheric pressure in determining the dynamically relevant subsurface pressure in the water column.

3. Results

3.1. Velocity patterns at the mainland and Islands are distinct

The mainland and the Islands have distinctly different water velocity patterns (Figure 3). On average, the circulation tends to be poleward along the mainland and eastward or very weak at the islands, though there is also strong variability in the flow on time scales of days. In summer, the flow is more strongly poleward (or weaker equatorward) at nearly all sites. North of Point Arguello at PTS and PUR, the mean flow is 0-5 cm/s, and weakens in summer. South of Point Arguello, except at JAL in the lee of a headland, the flow is stronger (0-10 cm/s) and strengthens in summer. At the Islands, the mean flow is generally eastward up to 12 cm/s or very weak (< 2 cm/s), with the strongest flows near headlands and inter-island channels. The one site with substantial westward flow is on the south side of Santa Cruz Island at VAL, adjacent to a deep basin (> 2000 m). There is a region of very weak mean flow variability on the north side of Santa Cruz Island, at PRO and PEL, as compared to other sites. Although the average directions of flow at the mainland and Islands are opposite, the entire region south of Point Conception makes an adjustment toward more poleward flow in summer. The summer-intensified poleward flow along the mainland south of Point Conception is a signature of buoyancy-driven coastal flows associated with relaxation of the prevailing upwelling-favorable winds [Cudaback et al. 2005, Melton et al. 2009]. At the Island sites, the mean flow also becomes more westward (or weaker eastward) in summer.

Everywhere except north of Point Conception, there is a pattern of more westward flow in summer months. The circulation at all sites varies strongly on time scales of days. The variability in the along-shelf flow is generally stronger than the average flow. North of Point Conception, that is true in every month (only the variability over the entire year is shown). On the mainland south of Point Conception, the variability is stronger than the mean during winter but not summer. The subtidal variability along the mainland weakens by about half in summer (not shown) when the mean flow strengthens. At the Islands, the mean flow is also weaker than the variability except at sites near headlands (BAY, BEA, SRS). The strong variability in the flow indicates the nearshore water circulation in the SCB is characterized by frequent flow relaxations and reversals on time scales of days, rather than by a consistent direction of along-shelf flow.

If the mean flow is in the same direction as the major principal axis, the depth-average cross-shelf velocity uda will be zero. The observed uda is very weak (< 1.5 cm/s in all months) at all sites except BEA and MKO, which are near headlands. Correspondingly, at sites with substantial mean flow (speed > 2 cm/s), the direction of the long-term mean flow vector uda is within 4 deg of the major principal axis direction except at those two sites near headlands (BEA, MKO; Table 1). Since the major principal axis direction will be along-isobath if the flow is geostrophic, this suggests the mean flow is nearly along-isobath except near headlands.

To determine whether the circulation over the entire region can be characterized by a few simple patterns, we calculated the empirical orthogonal functions (EOFs) of the depth-average along- shelf flow vda and the near-surface cross-shelf flow us (from the top good ADCP bin at each site). That EOF analysis yielded only one statistically separate circulation mode out of 32 modes (Figure 4a). That first EOF explains 24% of the overall subtidal velocity variance in us and vda at all sites combined, and up to 75% (64%) of the variance in vda (us) at particular sites (Figure 4b). Generally, the sites at which the EOF captures a substantial amount of variance are western sites exposed to the large-scale wind field and not sites in the lee of Point Conception. Because not all mainland and island sites had ADCP deployments that overlapped in time, all the ADCP sites cannot be included in a single EOF analysis. Nevertheless, the mode in Figure 4a is not sensitive to the choice of sites to include. A similar first EOF emerges if CAR, or BAY and BEA, are not included. Without BAY and BEA, it is possible to include MKO on the mainland; the results are similar to Figure 4, and the EOF amplitude at MKO is < 1 cm/s and explains none of the variance at MKO, similar to nearby sites. The only statistically unique EOF captures little of the flow variance in the eastern Channel.

3.2. Vertical profiles of velocity are consistent over the region

The long-term mean along-shelf velocity profile is surface-intensified at most sites, and constant vertically at the others. The along-shelf velocity is generally unidirectional: the velocity at each depth in the water column is in the same direction as the depth-average flow (Figure 5). Along the mainland (at the Islands) the velocities become more poleward (equatorward) with height above bottom. Flow speeds are 0-6 cm/s near the bottom and 0-10 cm/s near the surface. At mainland sites, the vertical shear in the along-shelf flow is strongest near the bottom and approaches zero near the surface (Figure 5, top). On the

north sides of the Islands, the shear is nearly constant throughout the water column so the profiles are more linear (Figure 5, bottom, open symbols). In general, the shear is less than 0.5 (cm/s)/m.

The variability in the subtidal along-shelf flow, as measured by its standard deviation at each ADCP bin depth, ranges from 1-10 cm/s and tends to be larger at sites and ADCP bin depths with larger mean flow speeds (r2 = 0.3 for correlation between flow speed and standard deviation). Seasonal variations in the along-shelf flow involve strengthening and weakening of the profiles in Figure 5 by a factor of about 2 or less, in accordance with the monthly arrows in Figure 2, without substantial changes in the profile shapes.

Surprisingly, nearly all the time-average profiles of cross-shelf flow are very similar (Figure 6). The profiles are C-shaped, with offshore or weak flow near the surface and bottom and onshore flow in the middle of the water column. The long-term mean vertical profiles of cross-shelf velocity are strikingly similar at 18 of the 21 sites. The cross-shelf velocities are weaker on the north sides of the Islands than at mainland or south Island sites. Generally, the cross-shelf flow is O(1 cm/s) or less at all depths except near headlands (BEA, which is off scale in Figure 6 left column; and MKO). The subtidal variability (standard deviation) in cross-shelf flow ranges from <0.5 cm/s at PEL north of Santa Cruz Island to 3 cm/s along the mainland. The main effect of seasonal variations is to strengthen and weaken the curvature of the cross-shelf flow profiles so the velocities vary by a factor of ~2 (not shown).

The cross-shelf flow profiles depend somewhat on the choice of coordinate system. The profile shapes in Figure 6 are not artifacts of uncertainty in the ADCP compass directions: the C-shapes are not sensitive to rotating the coordinate system +/-5 deg. The cross-shelf direction can be defined as the direction that has zero depth-average flow in the long-term time-average sense (Figure 6, right panels) or as the minor principal axis direction (Figure 6 left panels, and elsewhere in this manuscript). The cross-isobath direction is a third option, but sufficiently detailed bathymetry is not available. The cross-shelf flow profiles collapse better in the first coordinate system, as do similar profiles in the Middle Atlantic Bight [Lentz, 2008]. Three of the 21 sites (PUR, NAP, BEA) do not fit the C-shaped pattern in either coordinate system, and two (MKO, SCP) fit the pattern in one coordinate system but not the other. Those five sites are colored grey in Figure 6. Nevertheless, the C-shaped pattern is very robust.

3.3 Response to Wind

At western sites exposed to the prevailing equatorward winds, most of the variance in the flow is explained by local wind. The along-shelf flow vda and the near-surface and near-bottom cross- shelf velocities us and ub are significantly correlated with the wind stress at the 95% confidence level at most sites (Figures 7 and 8). At "exposed" sites in the western half of the study area, up to 60% of the velocity variance can be explained by local wind forcing alone, particularly at BAY and BEA for vda, and SRS and sites north of Point Conception for us and ub.

The sites where the flow is strongly correlated with the buoy winds in Figures 7 and 8 are generally the same sites that have substantial spatial amplitudes in the EOF mode shown in Figure 4. The time series amplitude of that EOF mode is strongly positively correlated with equatorward wind stress at buoys 46053 (r2 = 0.7) and 46054 (r2 = 0.6), suggesting the spatial pattern of that EOF is a good representation of the spatial pattern of response to wind forcing.

At sites in the lee of Point Conception in the eastern SBC, local wind explains little of the velocity variance (Figures 7 and 8). The water velocity at sheltered sites is generally not better predicted by the land-based wind stations (Figure 1) than by buoy 46053 or 46054, and even for sites where a land station does give a somewhat higher r2, the correlation of wind and flow is not strong (r2 <0.35). The circulation at sites in the lee of Point Conception is not well explained by local wind forcing.

The response of the cross-shelf flow to wind has a two-layered structure. The sign of the correlation of us and ub with wind stress is consistent with a two-layer coastal upwelling and downwelling circulation at all sites: equatorward wind stress fluctuations are associated with south/westward near-surface flow and north/eastward near-bottom flow (Figure 8). For example, when the wind at buoy 46054 is upwelling-favorable, at SMS the near-surface flow is directed offshore, the near-bottom flow is onshore, and the two velocities are highly correlated in time both with the wind stress (r2 = 0.5, Figure 8) and with each other (r2 = 0.5, Figure 9). The time average of each two-layered response contributes to the corresponding C-shaped profile (Figure 6) by turning the near-surface flow offshore.

3.4. Response to coastal sea-level gradient

The lack of correlation between flow and local wind at many sheltered sites (Figures 7 and 8) suggests nearshore flow in this region is strongly influenced by pressure gradients. The pressure gradients may be set up by the local topography or associated with the energetic mesoscale eddy field or with remotely-generated coastal-trapped waves, both of which influence the mid- and outer-shelf flow in the SBC [Auad and Hendershott, 1997]. With the exception of JAL in the lee of Point Conception, the mean flow along the mainland (Figure 3) opposes the large-scale wind stress (Figure 2) at all times of year, also indicating that local wind is not the only forcing influencing the along-shelf flow. Though the mean along-shelf pressure gradient is too small to observe, the poleward mean flow is consistent with the existence of a mean poleward pressure gradient force suggested in previous studies along the U.S. West Coast.

During weak winds ((|τ|<0.05 Pa) the average cross-shelf velocity profiles are J-shaped, rather than the C-shaped profiles during all wind conditions (Figure 6), consistent with flow driven by an alongshelf pressure gradient. Sea level gradients measured along the mainland coast (and transformed into synthetic subsurface pressure gradients) have a significant effect on velocity at the mainland but not Island sites. The effect of pressure gradient forcing is weaker poleward flow during equatorward sea-level anomalies, and stronger poleward flow during poleward sea level anomalies (Figure 10). Associated

with that poleward flow is enhanced offshore flow near the bottom of the water column, consistent with bottom Ekman layer dynamics.

To determine the effect of the fluctuating coastal ssp gradient (Δssp) between Port San Luis and Santa Monica on local flow, it is important to note that Δssp is itself negatively correlated with local wind forcing. The correlation squared of Δssp with poleward wind stress at buoy 46054 on subtidal time scales is a maximum of 0.36, for Δssp lagging wind stress by 15 hours. This indicates the observed Δssp fluctuations are ~35% a response to local wind, and not due only to mesoscale eddies or remotely-generated coastal-trapped waves. The effect of Δssp itself on the flow can be determined during weak wind forcing. During weak winds ($|\tau|<0.05$ Pa), the flow along the mainland is substantially different depending on the sign of the Δssp anomaly.

Conditionally-averaged patterns of depth-average flow for various wind and Δssp forcing states reveal several effects of wind and pressure gradient forcing. They are:

Strong equatorward (upwelling-favorable) wind stress at buoy 46053 in the eastern SBC is associated with equatorward flow everywhere in the domain, even within the wind shadow of Point Conception. During very strong poleward Δssp forcing, the mainland flow in the wind shadow is weak but not poleward.

Poleward (downwelling-favorable) wind stress, which occur mainly in winter, are associated with strongly poleward flow at mainland sites but not at the Islands. As the wind stress goes from equatorward to poleward the flow on the mainland changes from equatorward or zero flow to increasingly strong poleward flow at all sites. At the Islands, however, the strong equatorward flows at BAY, BEA, SRS, MOR, and SCP weaken but do not reverse (except weakly at SCP, and the southward component of flow at BEA does reverse to northward). The flow at the Islands is not strongly poleward for any combination of wind and Δssp forcing.

Poleward pressure gradient anomalies are associated with poleward flow along the mainland, except during strong equatorward wind stresses, which overcome the poleward pgf and result in equatorward flow along the mainland. During moderate equatorward winds a poleward pressure gradient force is still associated with poleward flow along the mainland.

Equatorward pressure gradient anomalies are not associated with equatorward flow along the mainland. Equatorward Δssp anomalies are associated with poleward flow along the mainland during weak wind stresses, and weak flow on the mainland during weak equatorward wind stresses. This is again consistent with previous studies suggesting a mean poleward pressure gradient force (pgf) exists on the U.S. West Coast. That mean pgf would be added to the Δssp anomaly observed here and is apparently strong enough to make the net pgf poleward at all times.

Near-zero Δssp anomalies are also associated with poleward flow along the mainland during weak wind stresses, and even weak equatorward wind stresses. This suggests the

mean pressure gradient force along the mainland is poleward, in accordance with previous studies of the Southern California Bight and West Coast of North America (as mentioned above).

The measured coastal pressure gradient anomaly has little effect on flow at the islands. The flow at some Island stations CUY, SMS, PRO, PEL, and VAL is weak even during wind forcing. This suggests the substantial flow that does at times exist at VAL (Figure 3) is not produced by either local wind (as represented by buoy 46053) or the coastal Δssp. The tendency of wind stress to drive flow in the direction of the wind stress is consistent for any value of Δssp, but the strength of the flow response is stronger at mainland sites than at Island site connection between flow at the mainland and flow at the Islands.

4. Conclusions

The presence of only one separate EOF out of 32 modes is in contrast to the Winant et al. (2003) study that focuses on the deeper SBC. The result indicates that the nearshore flow at the mainland and islands cannot be described as the combination of a few simple, distinct velocity patterns. The ~75% of the subtidal velocity variance not accounted for by EOF 1 is apparently not strongly coherent over the study area, suggesting different wind and pressure gradient forcing is important at different sites and/or local topography plays a dominant role in driving the nearshore flow. Furthermore, flow variability in the nearshore region exists with higher frequency than the synoptic to seasonal scales described by Winant et al. (2003).

References

Auad, G., and M. Hendershott, 1997: The low frequency transport in the Santa Barbara Channel: description and forcing, *Continental Shelf Research,* **17**,779-802.

Checkley, D.M., and J.A. Barth, 2009: Patterns and processes in the California Current System, *Progress in Oceanography*, **83**, 49-64.

Cudaback, C.N., L. Washburn, and E. Dever, 2005: Subtidal inner-shelf circulation near Point Conception, California, *J. Geophys. Res.,* **110**, C10007, doi:10.1029/2004JC002608.

Harms, S., and C.D. Winant, 1998: Characteristic patterns of the circulation in the Santa Barbara Channel, *J. Geophys. Res.,* **103**, 3041 – 3065.

Lentz, S.J., 2008: Seasonal Variations in the circulation over the Middle Atlantic Bight continental shelf, *J. Phys. Oceanogr.*, **38**, 1486–1500.

Melton, C., L. Washburn, and C. Gotschalk, 2009: Wind relaxations and poleward flow events in a coastal upwelling system on the central California coast, *J. Geophys. Res.,* **114**, C11016, doi:10.1029/2009JC005397.

Pawlowicz, R., R. C. Beardsley, and S. J. Lentz, 2002: Harmonic analysis including error estimates in MATLAB using T TIDE. *Computers and Geosciences.*

Smith, S.D., 1988: Coefficients for sea surface wind stress, heat flux and wind profiles as a function of wind speed and temperature. *J. Geophys. Res.,* **93**, 15,467–15,472.

Winant, C.D., E.P. Dever, and M.C. Hendershott, 2003: Characteristic patterns of shelf circulation at the boundary between central and southern California, *J. Geophys. Res.*, *108*(C2), 3021, doi:10.1029/2001JC001302.

site,	pa dir,	mean flow dir,	mf-pa dir,	mean flow speed (cm/s)
PTS	143	140	-3	2
PUR	137	133	-4	1
ARG	180	178	-2	6
JAL	127	131	4	3
ALE	183	180	-3	5
ARQ	166	166	-0	2
NAP	157	156	-1	6
ELL	163	147	-16	2
ARB	161	188	27	1
MK0	162	207	44	3
CAR	165	178	13	2
CUY	161	82	-78	1
BAY	144	146	2	8
CTN	183	179	-4	4
BEA	112	187	74	11
PR0	158	226	69	0
PEL	145	121	-24	1
SCP	146	258	113	1
SMS	178	139	-39	1
SRS	149	147	-2	6
M0R	141	159	19	2
VAL	200	198	-3	2

Table 1. Major principal axis (y) direction, measured in degrees CCW from due east; direction of the depth-average mean flow vector $\mathbf{u}_{da}$; difference in direction between the mean flow and principal axis; and speed of the mean flow, $|\mathbf{u}_{da}|$.

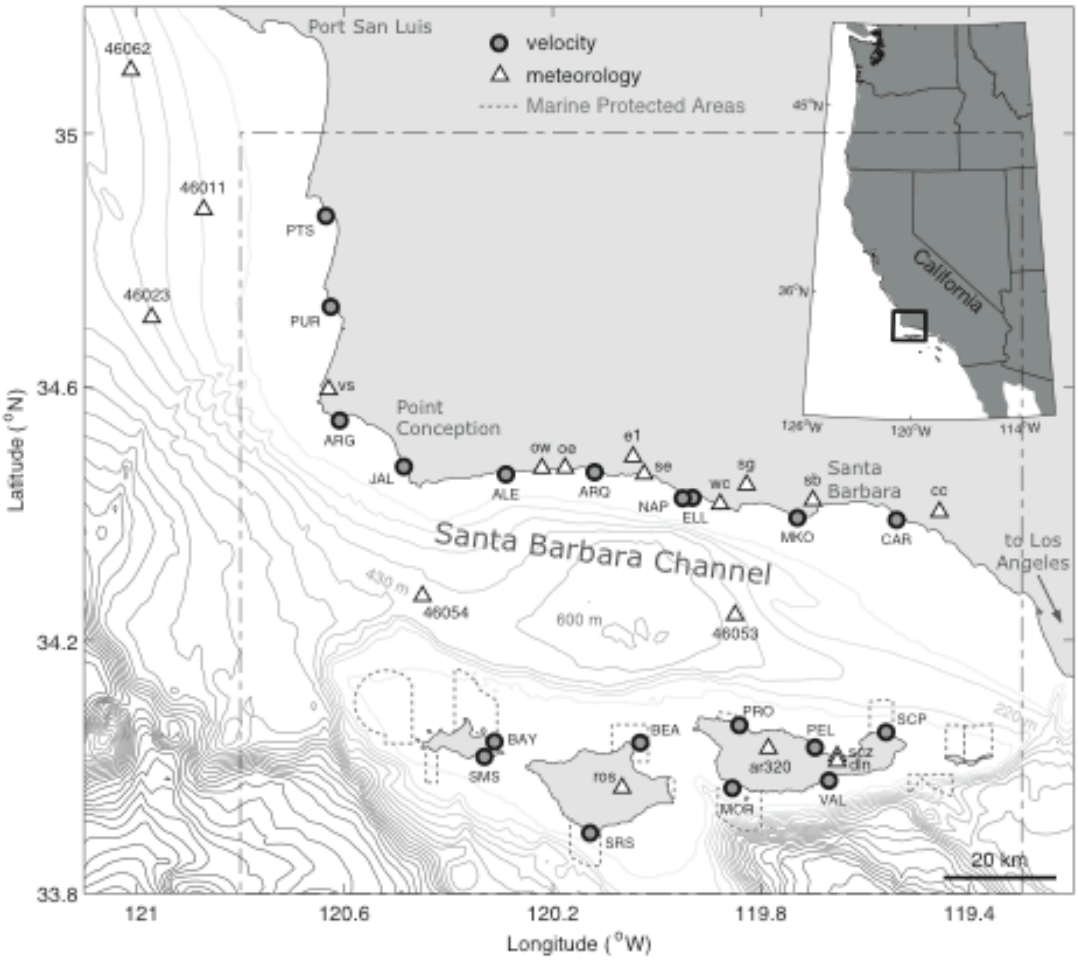

Figure 1. Map of study region near Point Conception, California. Isobaths are drawn every 100 m. The four Northern Channel Islands are, from west to east: San Miguel, Santa Rosa, Santa Cruz, and Anacapa. Large dashed box indicates area covered by maps in Figures 3 and after. Upper right: map of western United States; black rectangle indicates location of study region.

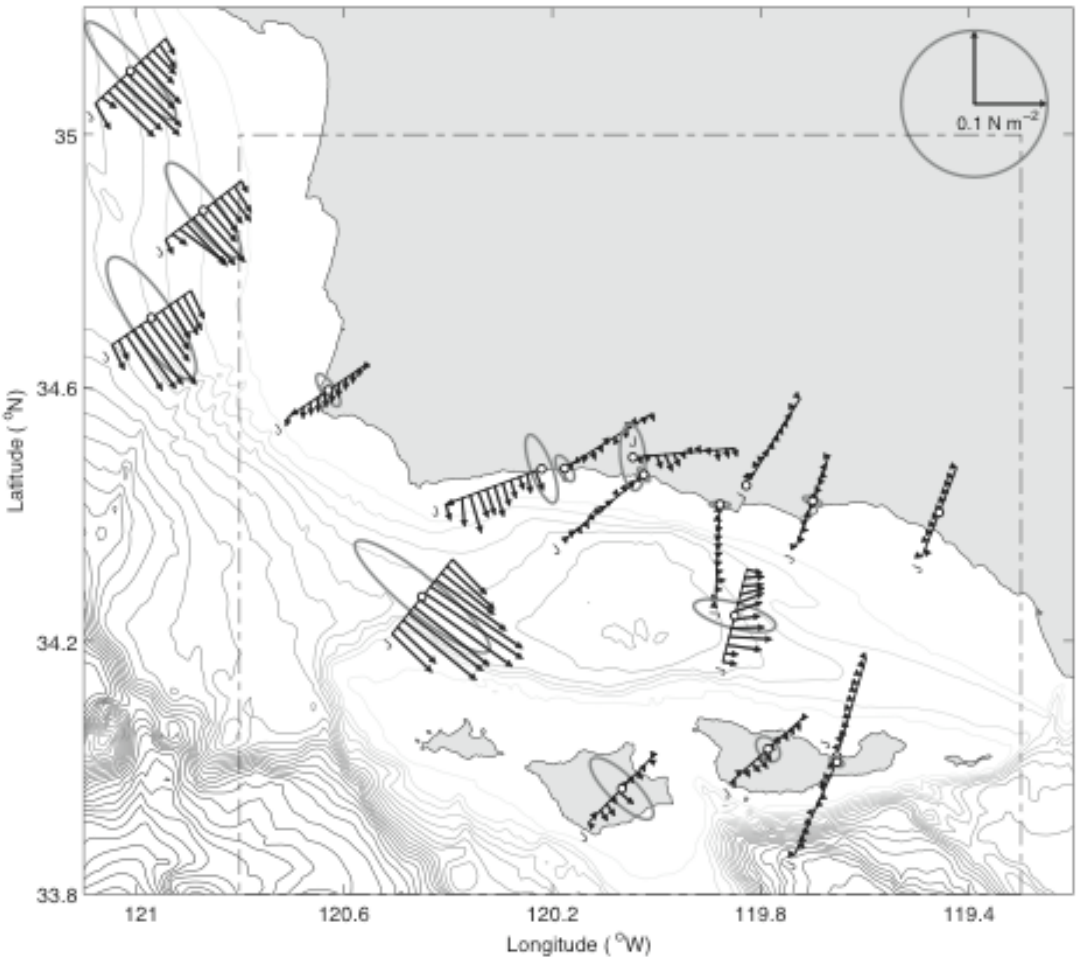

Figure 2. Time-mean wind stress (arrows) by month, and principal axis ellipses for 33-hr low- pass filtered wind stress, displayed as in Harms and Winant (1998). Dots with white centers indicate wind measurement locations. The baseline of the arrows is aligned with the minor principal axis (x) at each site. January is indicated by ``J''. Large dashed box indicates area covered by maps in Figures 3 and after.

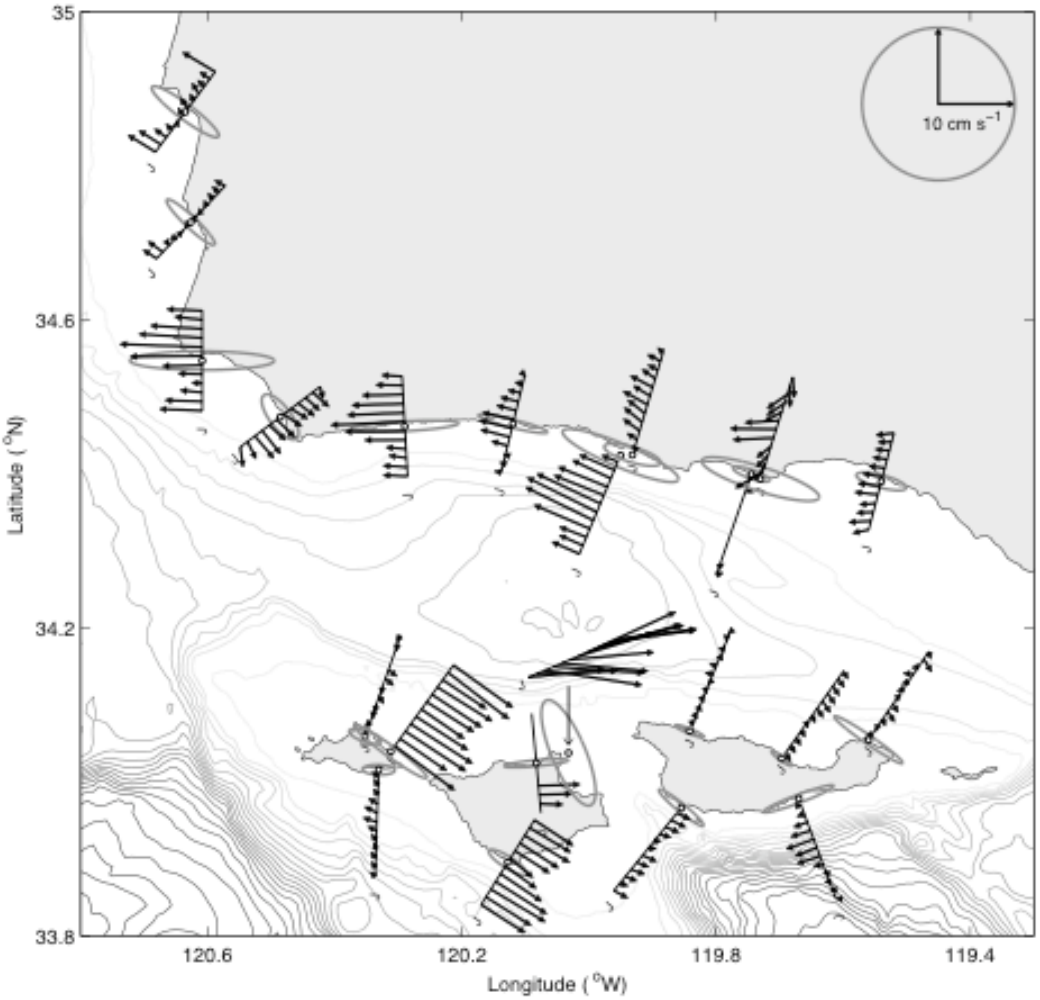

Figure 3. Time-mean, depth-average along-shelf flow (arrows) by month, displayed as in Harms and Winant (1998). Dots with white centers indicate mooring locations. The baselines of the arrows are aligned with the minor principal axis (x) at each site. January is indicated by ``J''. At each site, only months with at least three weeks of data are included. The semi-minor and -major axes of the principal axis ellipses (grey) indicate the standard deviations of the cross- and along- shelf flow.

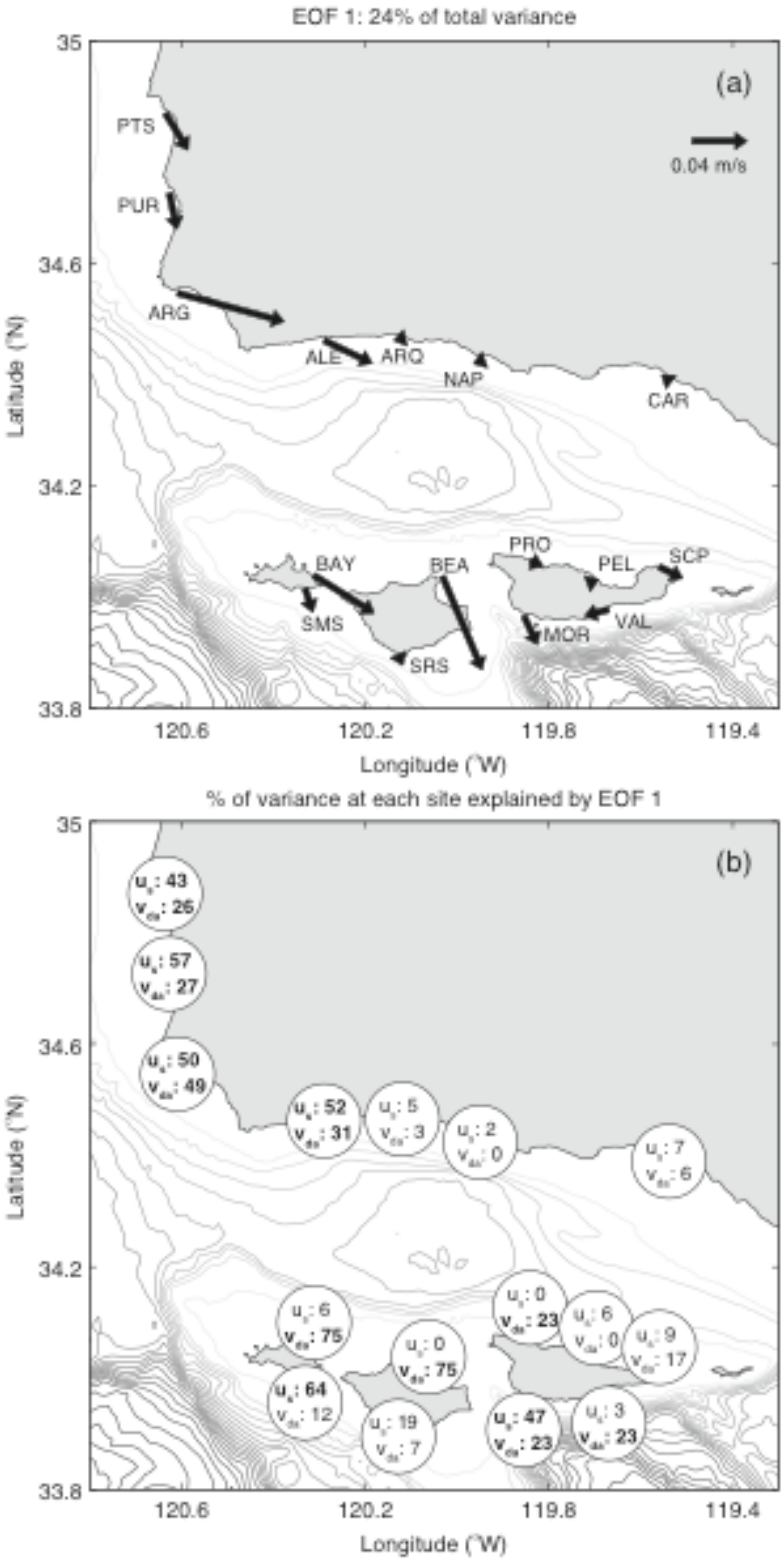

Figure 4. (a) Spatial pattern of first EOF of depth-average along-shore flow and near-surface cross-shore flow. (b) Percent of variance this EOF explains in each flow component at each site (bold if >20%).

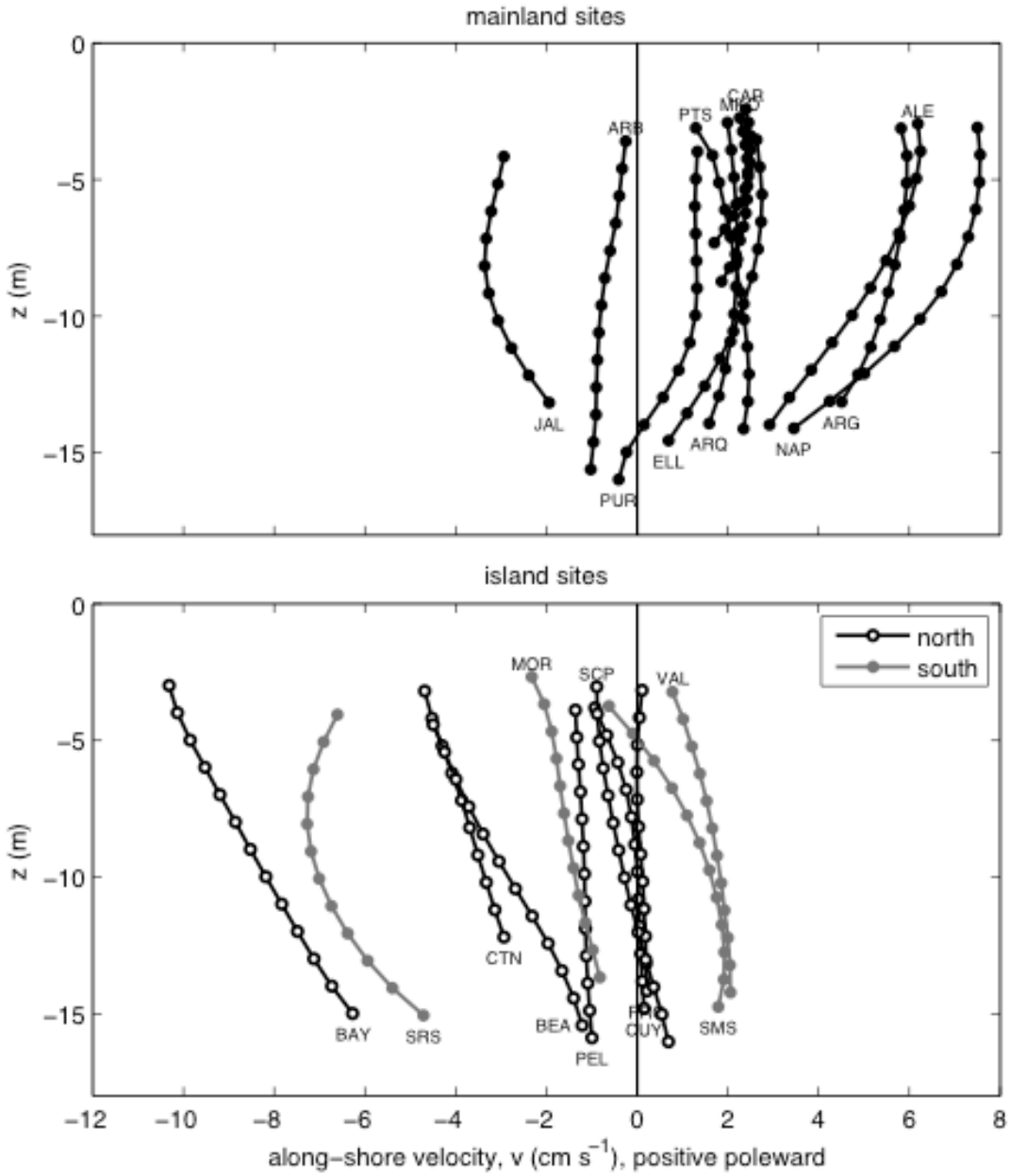

Figure 5. Vertical profiles of time-mean along-shore velocity at (top) mainland and (bottom) island sites.

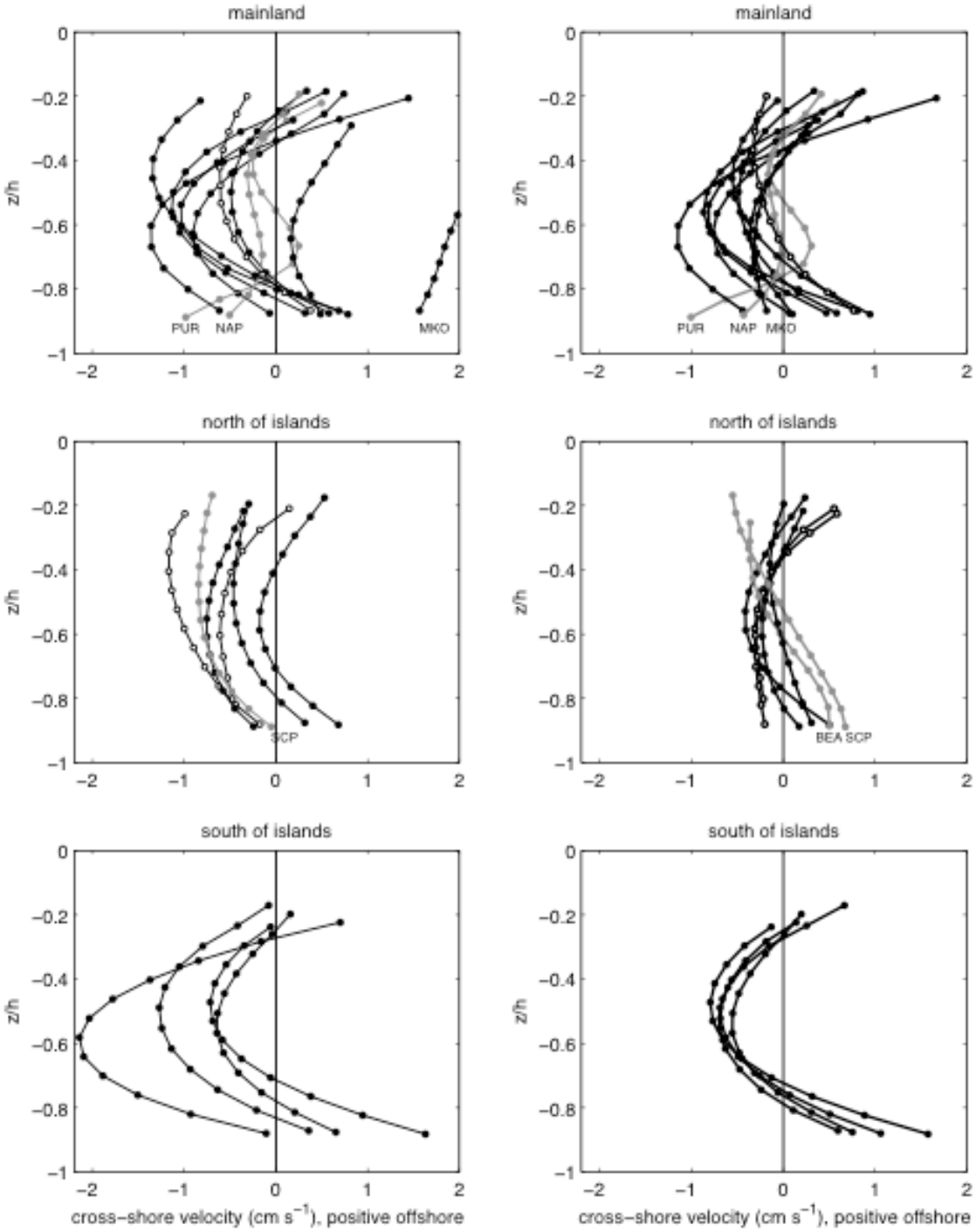

Figure 6. Vertical profiles of time-mean cross-shelf flow at all sites, in two coordinate systems. Left column: principal axes coordinates. Right column: The coordinate system that has uda = 0. Light grey profiles are sites that do not fit the C-shape pattern in both coordinate systems. Open symbols are sites with less than 2 years of data.

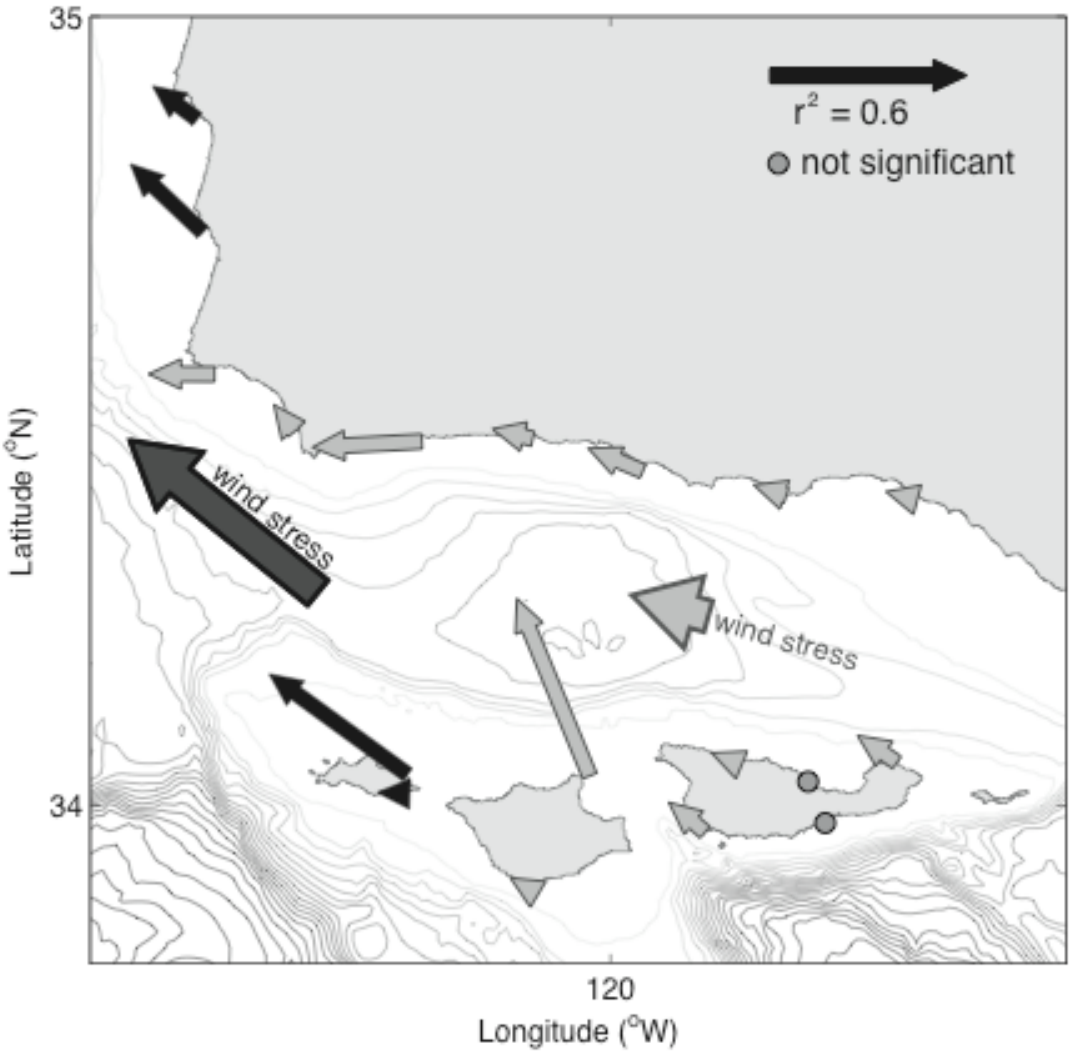

Figure 7. Correlation of depth-average along-shelf flow vda with local wind stress at buoy 46054 (black arrows) or 46053 (grey arrows), at zero lag. The tail of each arrow is at the location of an ADCP. Length of arrow indicates correlation coefficient squared (r2). Arrows are oriented parallel to the local major principal axis direction (y). Direction of arrow indicates the flow direction when the wind stress fluctuation is poleward (downwelling-favorable, as shown by thick arrows labeled "wind stress"). Wind buoys 4western and eastern thick arrows, respectively.

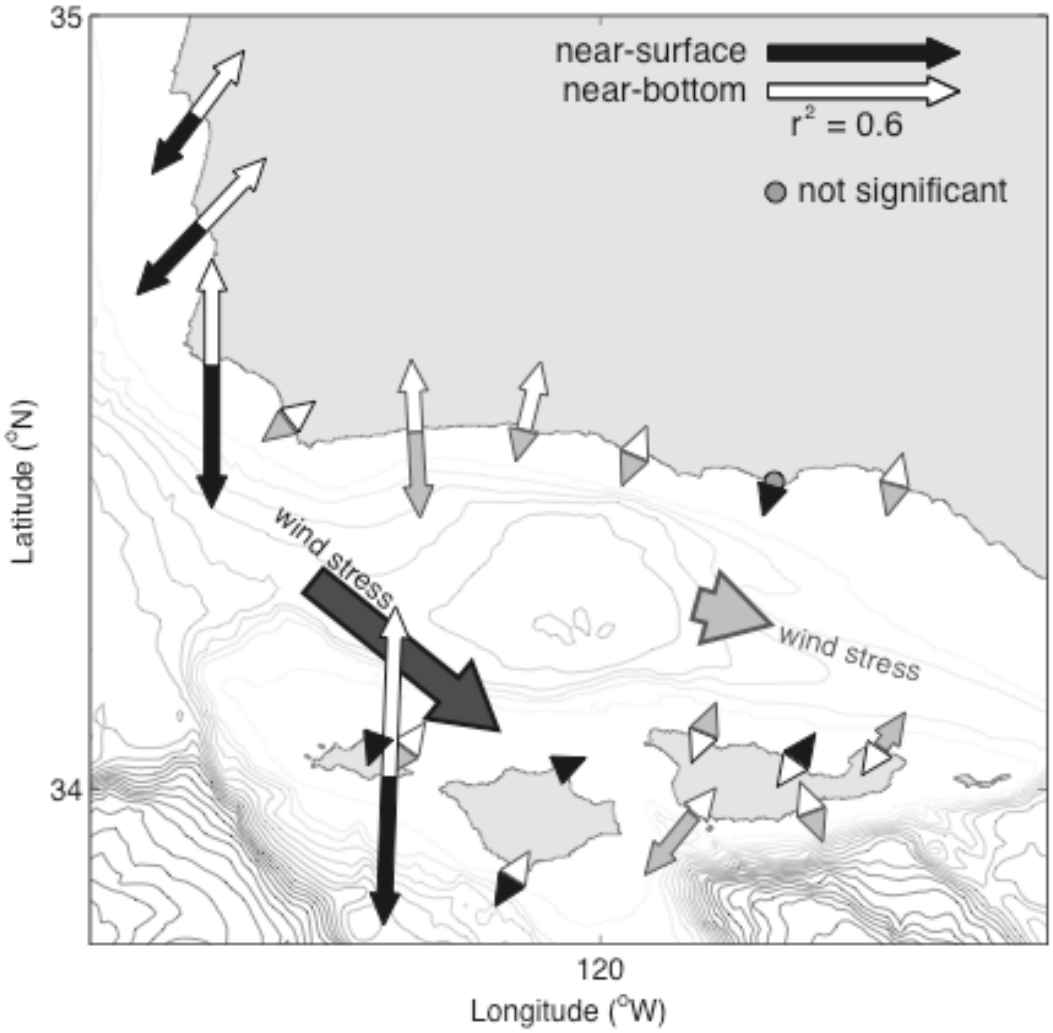

Figure 8. Correlation of near-surface cross-shelf flow us (filled arrows) and near-bottom cross- shelf flow ub (white arrows) with local wind stress at buoy 46054 (black) or 46053 (grey), at zero lag. The tail of each arrow is at the location of an ADCP. Length of arrow indicates correlation coefficient squared (r2). Arrows are oriented parallel to the local minor principal axis direction (x). Direction of arrow indicates the flow direction when the wind stress fluctuation is equatorward (upwelling-favorable, as shown by thick arrows labeled "wind stress"). Wind buoys 46054 and 46053 are located at the tails of the thick arrows.

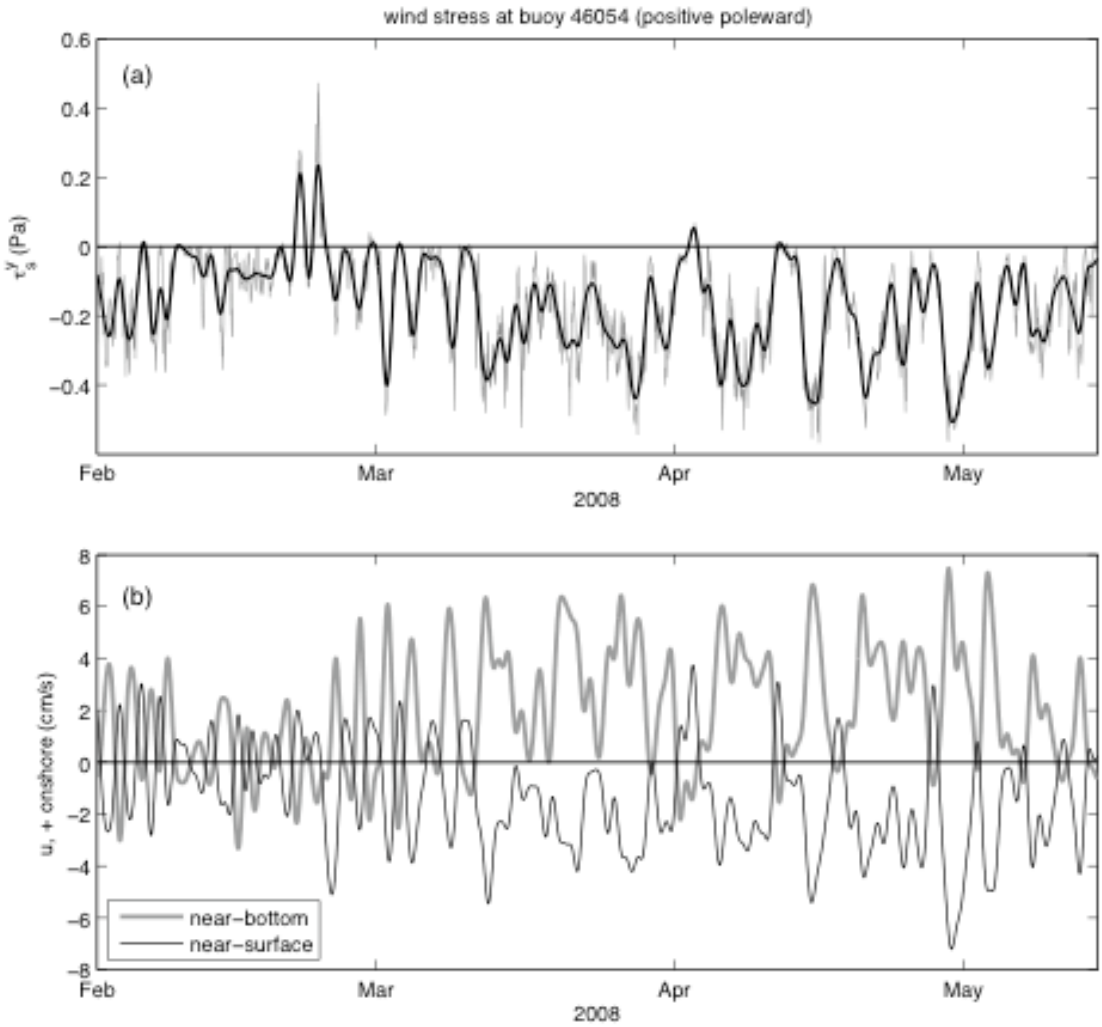

Figure 9. Example of relation of cross-shelf velocities near-surface and near-bottom to each other and to wind forcing. (a) y-component of wind stress (positive poleward) at buoy 46054, hourly (thin grey line) and low-pass filtered with a 33-hr cutoff (black line). (b) Cross-shelf velocities at SMS (positive onshore), low-pass filtered with a 33-hr cutoff. Grey: near-bottomADCP bin 2. Black line: near-surface velocity from top good ADCP bin.

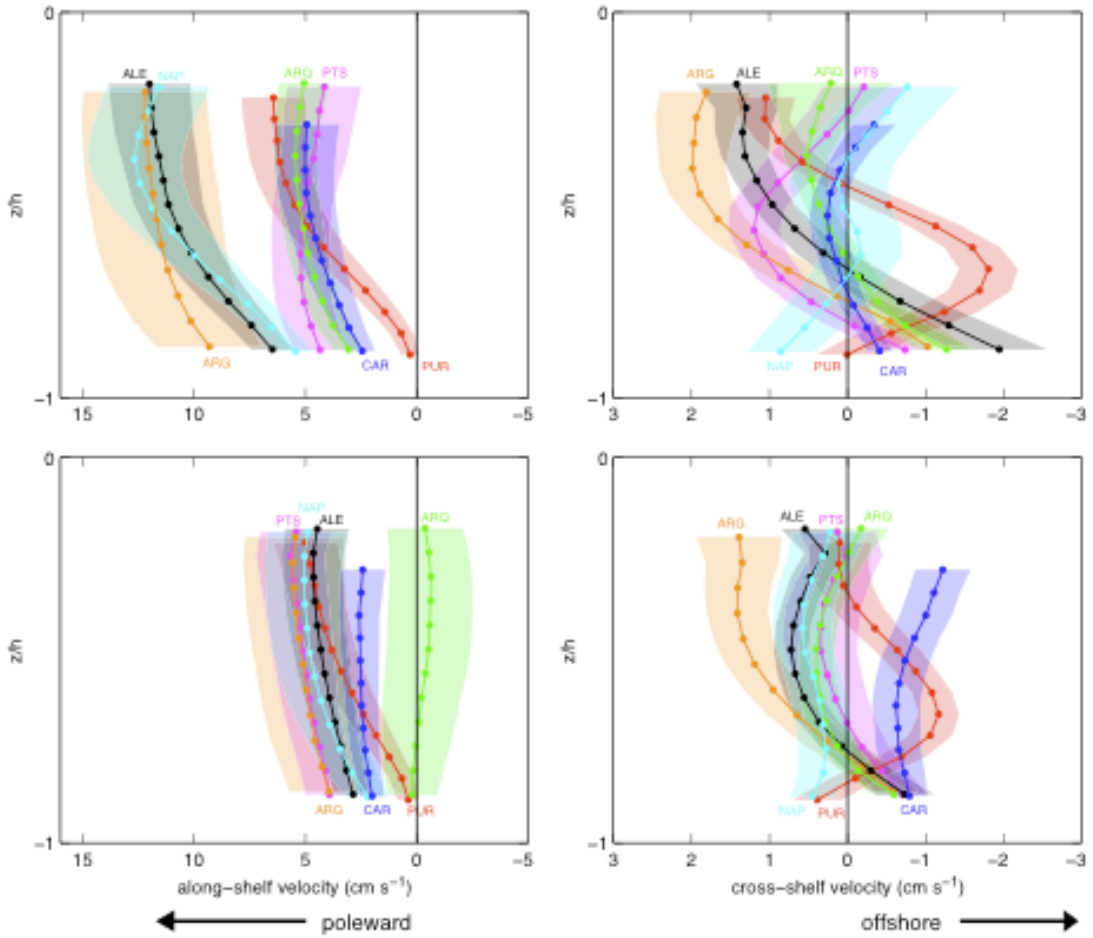

Figure 10. Velocity profiles along the mainland coast during weak winds (|τ|<.05 Pa) and (top) equatorward or (bottom) poleward pressure gradient force anomaly (|ΔSSPa| > 300 Pa). Left panels: along-shelf flow, positive poleward. Right panels: cross-shelf flow, positive onshore. For sites at the Islands, the profiles are not significantly different for the two pressure gradient cases.